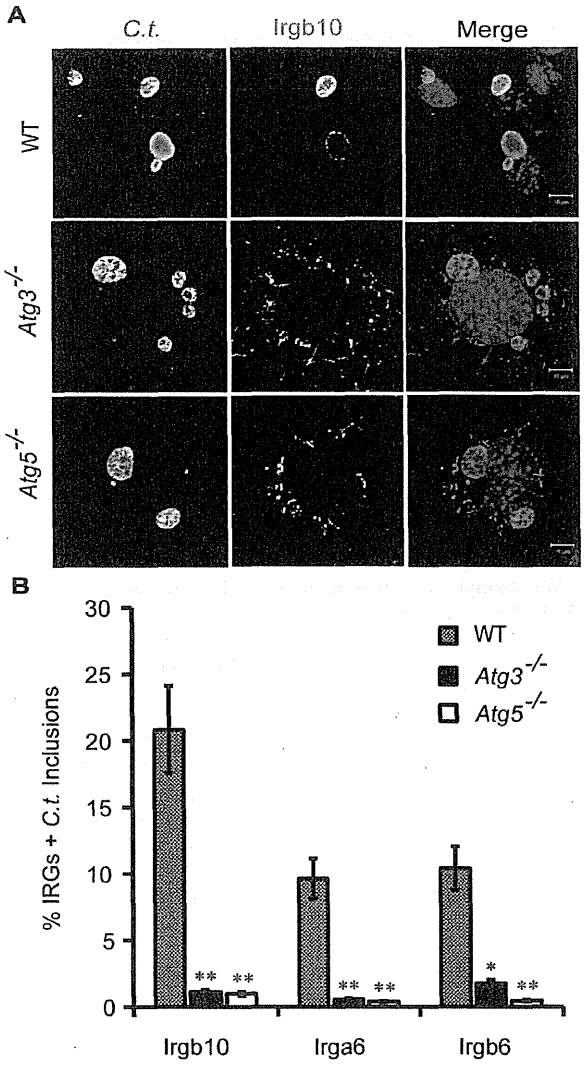


**Figure 2. Atg3 and Atg5 promote the delivery of GKS proteins to *C. trachomatis* inclusions.** (**A and B**) WT, *Atg3*$^{-/-}$ and *Atg5*$^{-/-}$ MEFs were infected with *C. trachomatis* and treated with 200 U/ml of IFNγ at 3 hpi. Cells were fixed at 20 hpi and stained with anti-*C. trachomatis* MOMP, anti-Irgb10, anti-Irga6, anti-Irgb6 and Hoechst. Representative staining with anti-Irgb10 is shown. (**B**) Colocalization of Irgb10, Irga6 and Irgb6 with inclusions in WT, *Atg3*$^{-/-}$ & *Atg5*$^{-/-}$ MEFs was quantified as described in Materials and Methods. The data are representative of three independent experiments. Error bars represent standard deviations. Statistical significance of group values relative to wildtype is shown (*, $p<0.05$, **, $p<0.005$).
doi:10.1371/journal.pone.0086684.g002

Atg8 protein family to the lipid phosphatidylethanolamine. Analogous to protein ubiquitination, this reaction is catalyzed by a set of enzymes with E1-, E2- and E3-like activities, termed Atg7, Atg3 and Atg5-Atg12 [26]. In addition to controlling the process of canonical macroautophagy, *Atg* genes have demonstrated roles in regulating additional cellular activities. These activities include, for example, the execution of alternative degradation pathways [27], the initiation of antimicrobial phagocytosis [28] and the inhibition of viral replication complexes [29]. Importantly, execution of these additional pathways frequently depends only on subsets, or *cassettes*, of canonical autophagy proteins [29]. For example, the shrinking of midgut cells during the development of *Drosophila* larvae has been shown to require Atg5 but not the E2-like conjugation enzyme Atg3 [30].

To better understand the role of autophagy-related genes in IFN-driven cell-autonomous immunity, we compared the ability of Atg5- and Atg3-deficient cells to execute IRG-/Gbp-dependent resistance to *T. gondii* and *C. trachomatis* infections. We found that Atg3, similar to Atg5, was required for cell-autonomous resistance and the efficient targeting of both GKS and Gbp proteins to PVs. The requirement for Atg5 and Atg3 in PV targeting could be overcome by expressing a dominant-active, GTP-bound form of the GKS protein Irgb10. These data suggest that Atg3-/Atg5-mediated Ubl lipidation may play a role in promoting GKS protein activation that is independent of the roles of Atg3 and Atg5 in degradative autophagy.

## Materials and Methods

### Host Cell Culture, Bacterial and Protozoan Strains and Infections

MEFs derived from wildtype (WT), *Atg3*$^{-/-}$, *Atg5*$^{-/-}$ and *Gbp*$^{chr3-/-}$ mice were previously described [31–33]. MEFs and African green monkey kidney Vero cells were cultured in Dulbecco's modified Eagle's medium supplemented with 10% heat-inactivated fetal bovine serum (FBS) (Denville and Life Technologies). *C. trachomatis* LGV-L2 were propagated as described [18]. A previously described GFP expression vector was transformed into *C. trachomatis*, as described [34]. GFP-expressing *Toxoplasma gondii* tachyzoites of the type II strain Prugniaud A7 and tachyzoites of the type II ME49 strain were propagated in Vero cells, as described [18] Infections with *C. trachomatis* were performed at a nominal multiplicity of infection of 1–5, as described [18]. For *T. gondii* infections cells were incubated overnight with or without 200 U/ml of IFNγ and asynchronously infected with tachyzoites at a nominal multiplicity of infection of 5–10.

### Immunocytochemistry

Immunocytochemistry was performed essentially as described previously [18]. Cells were washed thrice with PBS, pH 7.4 prior to fixation. Cells were fixed either with methanol or with 3% formaldehyde and 0.025% glutaraldehyde for 20 min at room temperature (RT). In all experiments involving formaldehyde/glutaraldehyde fixation, fixed cells were permeabilized/blocked with 0.05% (v/v) saponin and 2% BSA/PBS (SBP) for 30 min at RT. Then cells were stained with various primary antibodies, followed by Alexa Fluor-conjugated secondary antibodies (Molecular Probes/Invitrogen). Nucleic and bacterial DNA were stained with Hoechst 33258 according to the manufacturer's protocol. Stained cells were washed with PBS, mounted on microscope slides with FluorSave (Calbiochem) or ProLong Gold (Invitrogen), and allowed to cure overnight. Cells were imaged using either a Zeiss LSM 510 inverted confocal microscope or a Zeiss Axioskop 2 upright epifluorescence microscope. Colocalization of proteins with PVs was quantified in at least 3 independent experiments. In each experiment at least ten randomly selected fields were imaged for each experimental condition and cell type. To determine the frequency with which GKS and Gbp proteins colocalize with PVs, at least one hundred PVs were assessed for each experimental condition and cell type. Differential interference contrast images were used to identify extracellular *T. gondii* tachyzoites. The fraction of Gbp2- or Irgb10-positive vacuoles was determined for each field by dividing the number of Gbp2- or Irgb10-labeled

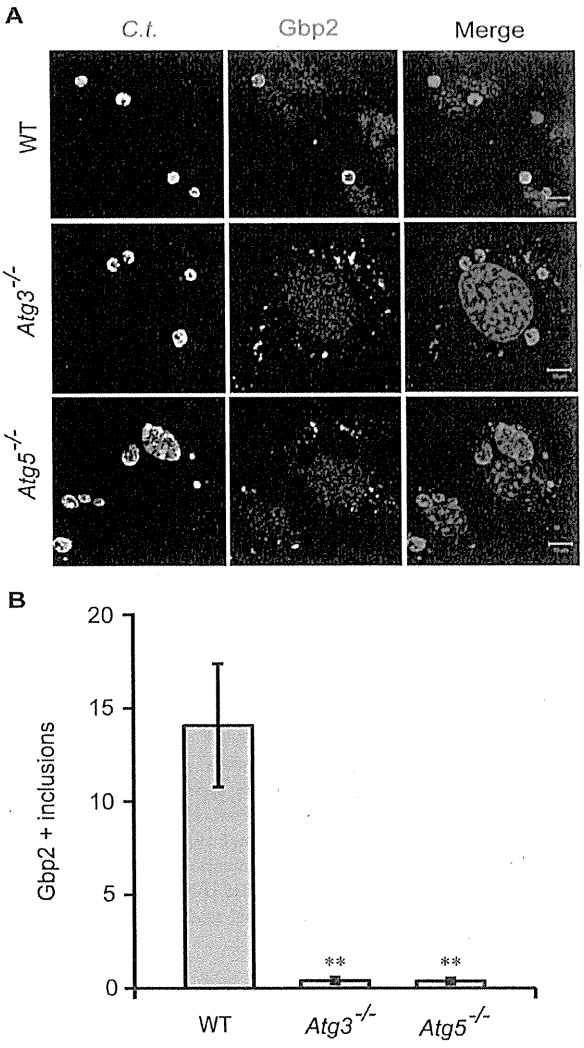


**Figure 3. Atg3 and Atg5 promote the efficient delivery of Gbp2 to *C. trachomatis* inclusions.** (**A**) WT, *Atg3*$^{-/-}$ & *Atg5*$^{-/-}$ MEFs were infected with *C. trachomatis* and treated with IFNγ at 3 hpi. Cells were fixed at 20 hpi and stained with anti-*C. trachomatis* MOMP, anti-Gbp2 and Hoechst. Representative images are shown. (**B**) Colocalization of Gbp2 with inclusions in WT, *Atg3*$^{-/-}$ and *Atg5*$^{-/-}$ MEFs was quantified as described in Materials and Methods. Error bars represent standard deviations of three independent experiments. Statistical significance of group values relative to wildtype is shown (**, $p<0.005$).
doi:10.1371/journal.pone.0086684.g003

vacuoles by the total number of vacuoles. Colocalization with *C. trachomatis* inclusions was quantified using the identical approach.

### Immunoblotting

Protein samples from whole cell lysates were analyzed by SDS-PAGE and Western blot, as described previously [18] Blots were probed with primary antibodies specific for: Atg3 (Abcam), Atg5 (Novus Biologicals), p62/SQSTM1 (MBL international), LC3 (MBL international), Gbp2, β-actin (Sigma). Binding of secondary HRP-labeled goat-anti-rabbit or goat-anti-mouse antibodies (Thermo Scientific) was analyzed using SuperSignal$^{(R)}$ West Pico or West Femto Chemiluminescent Substrate (Thermo Scientific).

### Antibodies

The primary antibodies used included anti-Gbp2 at 1:1000 [18], anti-Irga6 rabbit polyclonal antibody 765B0 [35] at 1:50000; anti-Irgb10 rabbit polyclonal antiserum [9] at 1:1000; anti-Irgb6 rabbit polyclonal antisera [35] at 1:1000; FITC-labeled mouse monoclonal anti-*C. trachomatis* MOMP [9] at 1:200; rabbit anti-IncG [36] at 1:50; anti-p62/SQSTM1 rabbit polyclonal antibody (MBL International) at 1:500; anti-LC3 rabbit polyclonal antibody (MBL International) at 1:1000; anti-Atg3 rabbit monoclonal antibody (Abcam) at 1:10000; anti-Atg5 rabbit polyclonal antibody (Novus Biologicals) at 1:500; and anti-*T. gondii* rabbit polyclonal antibody (Biogenex) at 1:500.

### Cell Transfection and Transduction

An Irgb10-GFP expression construct and the Irgb10$^{S82N}$ and Irgb10$^{K81A}$ mutants have been previously described [18]. MEFs were transfected using Attractene (Qiagen) following the manufacturers' instructions.

### Quantitative PCR

Total nucleic acid was prepared from trypsinized cell pellets using the QIAamp DNA Mini Kit from Qiagen (Valencia, CA USA). Samples were then subjected to singleplex qPCR on an ABI 7000 Sequence Detection System to assess the amount of 16s *Chlamydia* and GAPDH host DNA in the sample. *Chlamydia* 16s DNA was detected through use of the following primer sequences, essentially as described [37]: 16sforward primer 5′-GGA GGC TGC AGT CGA GAA TCT-3′, reverse primer 5′-TTA CAA CCC TAG AGC CTT CAT CAC A-3′, and dual-labeled probe 5′-[6-FAM]-TCG TCA GAC TTC CGT CCA TTG CGA-[TAMRA]-3′. Mouse GAPDH DNA was detected using the Rodent GAPDH Control Reagent Kit from Applied Biosystems (Foster City, CA, USA). Standard curves were generated in parallel from known amounts of *C. trachomatis* and murine DNA, and these curves were used to calculate the amount (pg) of *Chlamydia* DNA per unit mass (μg) of mouse DNA in the samples.

### Statistical Analysis

Results are represented as means ± SD. The unpaired two-tailed Student's t test was used to determine the statistical significance of the experimental data where $p \leq 0.05$ was considered significant.

## Results

### Atg3 and Atg5 Promote the Delivery of IFN-inducible GTPases to *T. gondii* PVs and *C. trachomatis* Inclusions

Targeting of GKS proteins to *T. gondii* PVs requires the expression of the autophagy protein Atg5 [24,25]. Autophagy is controlled by two Ubl conjugation systems: the first system conjugates the Ubl Atg12 to Atg5 and the second system conjugates the Ubl Atg8 (i.e. LC3 and its paralogs in mammalian cells) to lipids [26]. Only the Atg8 but not the Atg12 conjugation system requires the E2-like conjugating enzyme Atg3 and accordingly Atg5-Atg12 conjugates are still formed in *Atg3*$^{-/-}$ cells (Figure 1A). As expected, we observed that autophagy-deficient *Atg3*$^{-/-}$ cells and *Atg5*$^{-/-}$ cells did not generate lipidated LC3 (LC3-II) and instead accumulated p62 protein, a known substrate of the autophagic degradation pathway (Figure 1A).

To determine whether the formation of Atg5-Atg12 conjugates was sufficient to direct GKS proteins to *T. gondii* PVs, we monitored the localization of the GKS protein Irgb10 in *Atg3*$^{-/-}$ MEFs. We found that colocalization of Irgb10 with *T. gondii* PVs

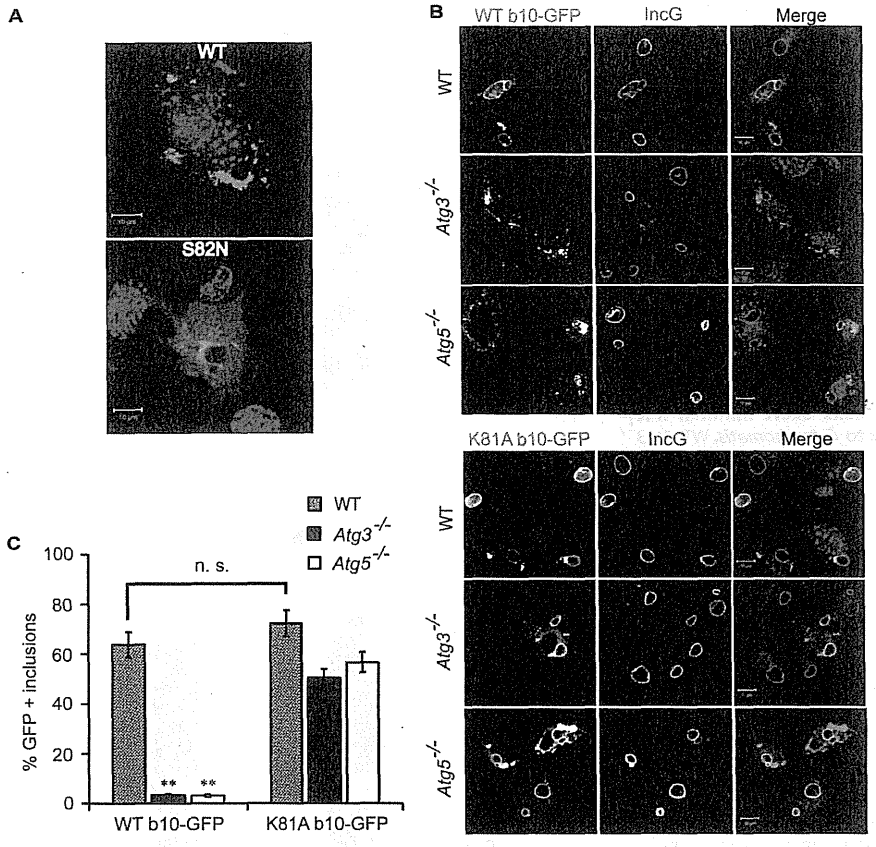


**Figure 4. GTP-locked Irgb10$^{K81A}$ mutant but not wildtype Irgb10 targets *C. trachomatis* inclusions in *Atg3*- and *Atg5*-deficient cells with high efficiency.** (**A**) *Atg5*$^{-/-}$ MEFs were transfected with GFP-fusion constructs expressing either wildtype Irgb10 (WT) or the Irgb10$^{S82N}$ mutant that is deficient of GTP binding. Cells were subsequently infected with *C. trachomatis* and treated with 200 U/ml of IFNγ at 3 hpi. Fixed cells were stained with Hoechst. Representative images are shown. (**B**) WT, *Atg3*$^{-/-}$ & *Atg5*$^{-/-}$ MEFs were transfected with the indicated constructs. Cells were infected with *C. trachomatis* and treated with IFNγ at 3 hpi. Cells were fixed at 20 hpi and stained for the *C. trachomatis* inclusion membrane marker IncG as well as DNA (Hoechst). Representative images are shown. (**C**) Graphical representation of the frequency at which WT Irgb10 and the Irgb10$^{K81A}$ mutant colocalize with inclusions. Average values ± SD of three independent experiments are shown. Differences in the targeting frequency for WT Irgb10 and Irgb10$^{K81A}$ to inclusions were evaluated for statistical significance (**, $p<0.005$).
doi:10.1371/journal.pone.0086684.g004

was diminished in *Atg3*$^{-/-}$ cells relative to wildtype cells (Figure 1B). Colocalization of the Gbp protein Gbp2 with *T. gondii* PVs was also reduced in *Atg3*$^{-/-}$ cells (Figure 1C). Overall the colocalization of Irgb10 and Gbp2 with *T. gondii* was reduced to similar levels in *Atg3*$^{-/-}$ and *Atg5*$^{-/-}$ MEFs (Figure 1D), suggesting that both of the two Ubl conjugation systems controlling autophagy are critical for the delivery and/or attachment of IFN-inducible GTPases to *T. gondii* PVs.

As previously reported, targeting of GKS proteins to *C. trachomatis* PVs, commonly referred to as *inclusions*, also requires Atg5 expression [22]. Here, we observed that the colocalization of the GKS proteins Irgb10, Irga6 and Irgb6 with inclusions was not only dependent on Atg5 but also on Atg3 expression (Figure 2 and Figure S1). Additionally, we found that endogenous Gbp2 was largely absent from *C. trachomatis* inclusions in both *Atg5*$^{-/-}$ and *Atg3*$^{-/-}$ cells (Figure 3). Collectively, these data show that Atg3 and Atg5 are both required for the efficient delivery of GKS and Gbp proteins to PVs formed by two distinct pathogens.

## The GTP-locked Irgb10-K81 Mutant Efficiently Targets *C. trachomatis* Inclusions and *T. gondii PVs* in Atg3- and Atg5-deficient Cells

The mechanism by which Atg5 controls the targeting of GKS proteins to PVs is unknown. One previously proposed model predicts that Atg5-dependent autophagy is required to maintain a pool of soluble, cytosolic GKS proteins available for PV targeting. This model is based on the observation that Atg5-deficient cells accumulate GTP-bound GKS protein aggregates in the cytosol [25] and the prediction that these protein aggregates would sequester GKS proteins away from PV targeting. To directly test whether GTP binding was necessary for the formation of GKS protein aggregates in *Atg5*$^{-/-}$ cells, we took advantage of the previously described Irgb10$^{S82N}$ mutant that is deficient for GTP binding [18]. We found that wildtype Irgb10 GFP-fusion proteins formed aggregates in *Atg5*$^{-/-}$ cells but Irgb10$^{S82N}$ GFP-fusion proteins did not (Figure 4A). These data indicate that GTP acquisition is required for the formation of Irgb10 protein aggregates in autophagy-deficient cells, as previously suggested [25]. We also observed the formation of Irgb10 protein aggregates in *Atg3*$^{-/-}$ cells (Figures 1 and 2), further supporting a possible

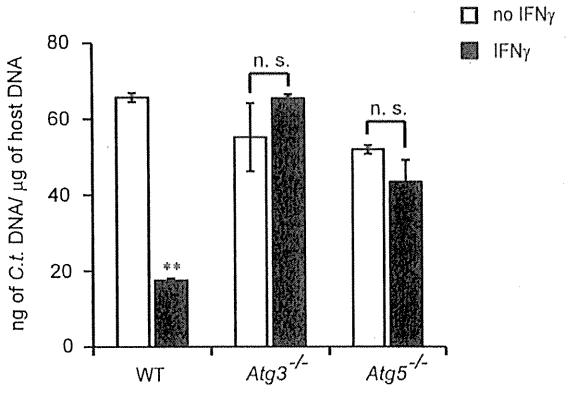


**Figure 5. *Atg3*- and *Atg5*-deficient cells exert minimal IFNγ-induced cell-autonomous resistance to *C. trachomatis*.** WT, $Atg3^{-/-}$ and $Atg5^{-/-}$ MEFs were either treated overnight with 200 U/ml of IFNγ or remained untreated. Cells were then infected with *C. trachomatis* for 24 h and total DNA was harvested for each biological sample. Chlamydial DNA was quantified by qPCR as described in Methods and Materials. Data are representative of three independent experiments. Statistical significance of group values between untreated and IFNγ-treated cells is shown (**, $p<0.005$; n. s. – not significant).
doi:10.1371/journal.pone.0086684.g005

model in which a defect in autophagic clearance of cytosolic GTP-bound GKS protein oligomers results in the formation of GKS protein aggregates. However, these results failed to determine whether or not aggregate formation causes the prevalent PV targeting defect observed in $Atg5^{-/-}$ and $Atg3^{-/-}$ cells.

Irgb10 protein aggregates form not only in $Atg5^{-/-}$ and $Atg3^{-/-}$ but also in *Irgm1/m3* cells. However, in *Irgm1/m3* cells Irgb10 targets *C. trachomatis* inclusions with high efficiency [18]. Therefore, Irgb10 aggregate formation seemed unlikely to be the cause for the Irgb10 targeting defect observed in $Atg5^{-/-}$ and $Atg3^{-/-}$ cells. Hence, we considered an alternative model in which Atg3 and Atg5 would play a more direct role in facilitating Irgb10 binding to PV membranes. Because the transition of Irgb10 into the GTP-bound, active state is a prerequisite for Irgb10 PV membrane binding [18], we considered that Atg3 and Atg5 could be involved in promoting Irgb10 activation. Therefore, we hypothesized that a GTP-locked, constitutively active Irgb10 mutant should target *C. trachomatis* independently of Atg3 and Atg5. To test this hypothesis, we ectopically expressed GFP-fusions of wildtype Irgb10 and the previously described GTP-locked mutant $Irgb10^{K81A}$ [18] and monitored their subcellular localization. We found that both Irgb10 variants localized to inclusions with comparable frequency in wildtype cells (Figures 4B and 4C). In *Atg3*- and *Atg5*-deficent cells, however, ectopically expressed Irgb10, similar to endogenous Irgb10, failed to localize to inclusions (Figures 4B and 4C). In contrast to wildtype Irgb10, the GTP-locked $Irgb10^{K81A}$ mutant localized to inclusions formed in $Atg5^{-/-}$ and $Atg3^{-/-}$ cells at high frequency (Figure 4B and 4C). $Irgb10^{K81A}$ but not wildtype Irgb10 similarly localized to *T. gondii* PVs in $Atg5^{-/-}$ and $Atg3^{-/-}$ cells (Figure S2), demonstrating that constitutive-active Irgb10 can target PVs formed by different pathogens independently of Atg5 and Atg3. Colocalization of $Irgb10^{K81A}$ with PVs occurred in spite of Irgb10 protein aggregate formation (Figure 4B and Figure S2). Therefore, the formation of GTP-bound Irgb10 aggregates is not sufficient to explain the failure of endogenous Irgb10 to target inclusions in $Atg5^{-/-}$ and $Atg3^{-/-}$ cells. Instead, our data suggest a possible involvement for

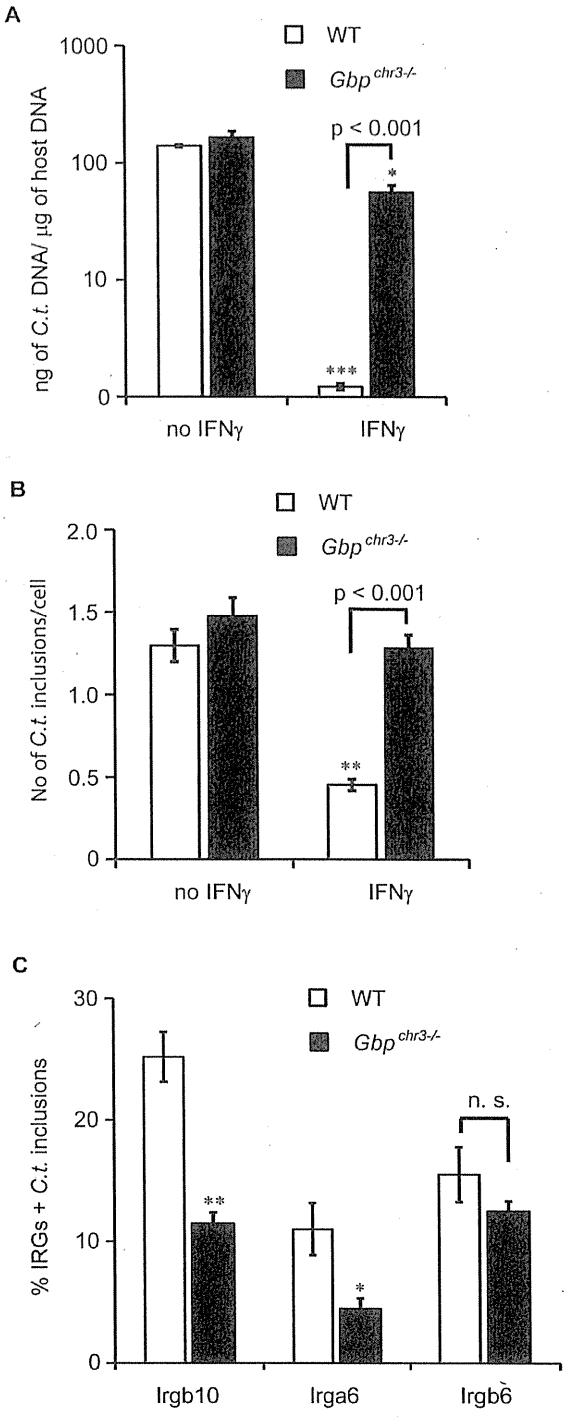


**Figure 6. A cluster of Gbp proteins on mouse chromosome 3 provides cell-autonomous resistance to *C. trachomatis* infections.** (**A**) WT and $Gbp^{chr3-/-}$ MEFs were either treated overnight with 200 U/ml of IFNγ or left untreated and subsequently infected with *C. trachomatis* for 24 h. Bacterial burden was assessed by qPCR as described in Methods and Materials. Data are representative of three independent experiments. Statistical significance of group values between untreated and IFNγ-treated cells is shown (*, $p<0.05$; ***, $p<0.005$). (**B**) WT and $Gbp^{chr3-/-}$ MEFs were infected with GFP-

expressing *C. trachomatis*, left untreated or treated with IFNγ at 3 hpi. Cells were fixed at 20 hpi and stained with Hoechst. The number of *C. trachomatis* inclusions per cell was measured. Data are representative of three independent experiments. Graph represents average values ± SD. Statistical significance of group values between untreated and IFNγ-treated cells is shown (**, $p<0.005$). (**C**) WT and $Gbp^{chr3-/-}$ MEFs were infected with GFP-expressing *C. trachomatis* and treated with IFNγ at 3 hpi. Cells were fixed at 20 hpi and stained with anti-Irgb10, anti-Irga6, anti-Irgb6 and Hoechst. Colocalization of Irgb10, Irga6 and Irgb6 with inclusions in WT, $Atg3^{-/-}$ & $Atg5^{-/-}$ MEFs was quantified as described in Materials and Methods. Error bars represent standard deviations of three independent experiments. Statistical significance of group values relative to wildtype is shown (*, $p<0.05$, **, $p<0.005$).
doi:10.1371/journal.pone.0086684.g006

Atg3 and Atg5 in promoting the transition of Irgb10 into the GTP-bound active state.

### Atg3 and Atg5 are Required for IFNγ-induced Cell-autonomous Resistance to *C. trachomatis* Infections

Because Atg3- and Atg5-deficient cells failed to efficiently deliver GKS proteins like Irgb10 to inclusions, we monitored the ability of these cells to restrict intracellular chlamydial growth following IFNγ activation. As our wildtype control we used $Atg3^{+/+}$ MEFs derived from $Atg3^{-/-}$ embryo littermates. Whereas IFNγ-activated wildtype cells significantly reduced bacterial burden relative to untreated controls, $Atg3^{-/-}$ cells had lost their ability to restrict chlamydial growth (Figure 5). As shown previously [22], we also observed a defect in $Atg5^{-/-}$ cells to contain bacterial burden upon IFNγ activation (Figure 5), demonstrating the importance for both Atg3 and Atg5 in cell-autonomous immunity to *C. trachomatis* infections.

### A Cluster of Gbp Proteins on Mouse Chromosome 3 Provides Cell-autonomous Resistance to *C. trachomatis* Infections

We next asked whether the failure of $Atg5^{-/-}$ and $Atg3^{-/-}$ cells to restrict chlamydial growth upon IFNγ activation could in part be caused by the inability of these cells to target Gbp proteins to inclusions and thus to execute Gbp-mediated cell-autonomous immunity. To test this hypothesis, we obtained $Gbp^{chr3-/-}$ MEFs that are deficient for a cluster of mouse *Gbp* genes encoded on mouse chromosome 3 [33]. This cluster encompasses the genes *Gbp1*, *Gbp2*, *Gbp3*, *Gbp5* and *Gbp7*. We stimulated $Gbp^{chr3-/-}$ and littermate-derived control MEFs with IFNγ over night and subsequently infected these cells with *C. trachomatis* for 24 hours. While IFNγ activation lowered bacterial burden in control MEFs by approximately 2 logs, IFNγ-activated $Gbp^{chr3-/-}$ MEFs reduced bacterial burden minimally compared to wildtype cells (Figure 6A). To gain a better understanding of the kinetics of Gbp-mediated cell-autonomous immunity towards *C. trachomatis*, we activated MEFs with IFNγ at 3 hours post-infection (hpi). We found that immune activation at 3 hpi resulted in a significant decrease in the number of inclusions in wildtype MEFs but failed to reduce the number of inclusions in $Gbp^{chr3-/-}$ MEFs (Figure 6B). These data suggest that Gbp proteins help execute resistance pathways that can target established *C. trachomatis* inclusions.

Because it was previously reported that Gbp proteins augment the colocalization of GKS proteins with *T. gondii* PVs [33], we explored whether Gbp proteins also promote GKS protein association with *C. trachomatis* inclusions. We found that the frequency of Irgb10 and Irga6 but not Irgb6 colocalization with inclusions was moderately reduced in $Gbp^{chr3-/-}$ cells (Figure 6C). Therefore, failure to retain GKS proteins at the inclusion may in part explain the loss of cell-autonomous immunity in $Gbp^{chr3-/-}$ cells.

## Discussion

Amongst the most abundantly expressed IFN-inducible proteins are GTPases of the IRG and Gbp families. The robust expression of these GTPases in immune-activated host cells immediately suggested a potential role for these proteins in providing resistance to infections. This obvious assumption was convincingly confirmed with the engineering and initial characterization of mice deficient for the IRG genes *Irgm1* and *Irgm3* [10,38]. Mice lacking either *Irgm1* or *Irgm3* individually or both simultaneously were found to be more susceptible to infections with the protozoan pathogen *T. gondii* as well as the bacterial pathogen *C. trachomatis* [9,10,38–40]. More recently, genetic deletions of individual *Gbp* genes as well as the deletion of the *Gbp* gene cluster on chromosome 3 demonstrated the importance of this second GTPase family in resistance to *T. gondii* infections [25,33,41,42]. Here, we demonstrate that Gbp proteins also provide resistance to *C. trachomatis* infections in mouse cells. Because human Gbp proteins were previously shown to restrict intracellular chlamydial replication [43,44], our data suggest that Gbp-mediated immunity directed against *C. trachomatis* may be conserved between mice and humans.

Both in human and mouse cells Gbp proteins associate with *C. trachomatis* inclusion membranes [18,43,44]. Similar to the behavior of Gbp proteins, the GKS group of IRG proteins binds to inclusion membranes as well as PV membranes surrounding *T. gondii* [9,22,45,46]. Gbp and GKS proteins colocalize at PVs [33,47] and several lines of evidence indicate that Gbp and GKS proteins promote each other's association with PVs [18,33]. In further support of these previous results, we show here that a subset of GKS proteins target inclusions with diminished efficiency in $Gbp^{chr3-/-}$ cells. Although the mechanism by which these two protein families influence one another's subcellular localization is currently unknown, these observations may suggest the existence of one or more PV targeting pathways that are shared between GKS and Gbp proteins.

The concept that Gbp and GKS proteins may be recruited to PVs by overlapping or identical cellular pathways is further supported by previous reports demonstrating that GKS and Gbp proteins both require Atg5 expression in order to efficiently associate with PVs [22–25]. While the importance for Atg5 in directing Gbp and GKS proteins to PVs is now well established, the mechanism by which Atg5 promotes the association of IFN-inducible GTPases with intracellular pathogens has remained largely unexplored. Here, we demonstrate that Gbp and GKS translocation to PVs also requires Atg3, the E2-like conjugation enzyme essential for the lipidation of Atg8 proteins. These data therefore indicate that Atg8-lipidation is essential to target members of both families of IFN-inducible GTPases to PVs.

The mammalian Atg8 protein family consists of seven homologs that can be grouped into three subfamilies: LC3, GABARAP and GATE-16. Similar to LC3, GABARAP and GATE-16 exist as both non-lipidated and lipidated forms, of which the latter ones associate with autophagosomes [48]. Once covalently linked to lipids, different Atg8 homologs appear to fulfill partly distinct, non-redundant functions in cargo recognition, autophagosome biogenesis and autophagosome maturation [48]. In addition to their roles in the execution of autophagy, Atg8 proteins have also been implicated in non-autophagic functions, which include intra-Golgi transport and unconventional secretion of proinflammatory cytokines [49–51]. At least some of these "alternative," non-autophagic functions are also dependent on the Atg8 lipidation

machinery [49]. Therefore, unsuspected phenotypes observed in $Atg5^{-/-}$ and $Atg3^{-/-}$ cells should be interpreted with caution, as they may not always be the result of a defective autophagic process. Indeed, as previously noted, the failure of $Atg5^{-/-}$ cells to deliver the GKS protein to PVs is not satisfactory explained with a defect in autophagy [24].

IFN activation of autophagy-deficient cells results in the formation of cytosolic GKS protein aggregates [24]. These aggregates appear to be composed of GTP-bound proteins, as detected by the use of a conformation-specific anti-Irga6 antibody [25]. In agreement with these previous observations, we show that GTP acquisition is necessary for aggregate formation in $Atg5^{-/-}$ cells. Similar to $Atg5^{-/-}$ cells, IRGM-deficient cells also accumulate aggregate-like GKS punctae that are composed of GTP-bound proteins [18,19,35]. However, critically distinct from the cytosolic GKS aggregates formed in $Atg5^{-/-}$ cells [25], GKS punctae formed in IRGM-deficient cells are membrane bound [18]. These observations imply distinct functions for Atg5 and IRGM proteins in regulating GKS activities. Strong experimental evidence indicates that membrane-bound IRGM proteins act as GDIs for GKS proteins and thereby block GKS binding to IRGM-decorated membranes [18,19]. In the absence of IRGM proteins, GKS proteins can bind to these IRGM-stripped membranes [18]. In $Atg5^{-/-}$ cells on the other hand, GKS aggregates form in the cytosol [25], suggesting that the presence of Atg5 favors the activation of GKS proteins at membranes. Atg5 may do this in two ways: 1) by clearing GTP-bound GKS proteins from the cytosol and 2) by retaining GKS proteins at Atg8-decorated membranes and promoting GKS protein activation at these target membranes. In this study we provide data in support of a possible role for Atg5 and Atg3 in GKS protein activation. We show that the constitutive active, GTP-locked mutant form of Irgb10, $Irgb10^{K81A}$, colocalizes with *C. trachomatis* inclusions and *T. gondii* PVs in $Atg5^{-/-}$ and $Atg3^{-/-}$ cells. The substantial rescue of PV targeting by $Irgb10^{K81A}$ is not merely the result of protein overexpression, since overexpression of wildtype Irgb10 fails to target PVs in the absence of Atg3 and Atg5. Because $Irgb10^{K81A}$ is no longer strictly dependent on Atg3 and Atg5 as cofactors for PV targeting, we propose a possible role for Atg3 and Atg5 in GKS protein activation. Although Atg3 and Atg5 may mediate such an activation step directly, it appears more likely that lipidated Atg8 proteins are required for tethering GKS proteins to PV membranes resulting in GKS activation at the target membrane. Future studies will address whether one or more specific Atg8 proteins are required for GKS targeting to PVs.

## Supporting Information

**Figure S1 Atg3 and Atg5 promote the delivery of GKS proteins Irga6 and Irgb6 to *C. trachomatis* inclusions.** WT, $Atg3^{-/-}$ and $Atg5^{-/-}$ MEFs were infected with *C. trachomatis* and treated with 200 U/ml of IFNγ at 3 hpi. Cells were fixed at 20 hpi and stained with Hoechst, anti-*C. trachomatis* MOMP, and anti-Irga6 or anti-Irgb6, respectively. Confocal immunofluorescence images are shown.
(TIF)

**Figure S2 GTP-locked $Irgb10^{K81A}$ mutant but not wild-type Irgb10 targets *T. gondii* PVs efficiently in *Atg3*- and *Atg5*-deficient cells. (A)** WT, $Atg3^{-/-}$ & $Atg5^{-/-}$ MEFs were transfected with the indicated constructs and treated with 200 U/ml of IFNγ overnight. Cells were infected with the *T. gondii* type II strain ME49 for 3 hours and stained with a polyclonal anti-*T. gondii* antibody as well as Hoechst. Representative images are shown. **(B)** Graphical representation of the frequency at which WT Irgb10 and the $Irgb10^{K81A}$ mutant colocalize with *T. gondii* PVs. Average values ± SD of three independent experiments are shown. Differences in the targeting frequency for WT Irgb10 and $Irgb10^{K81A}$ to inclusions were evaluated for statistical significance (*, $p<0.05$).
(TIF)

## Acknowledgments

We are thankful for the generous gift of immortalized $Atg3^{-/-}$ and control by MEFs by Dr. Masaaki Komatsu and a *Chlamydia*-adapted GFP expression vector by Dr. Ian Clarke. We would also like to thank Dr. Gregory Taylor for scientific advice and helpful comments on the manuscript.

## Author Contributions

Conceived and designed the experiments: AKH JC. Performed the experiments: AKH. Analyzed the data: AKH JC. Contributed reagents/materials/analysis tools: ASP DMP MY. Wrote the paper: JC.

## References

1. Randow F, MacMicking JD, James LC (2013) Cellular self-defense: how cell-autonomous immunity protects against pathogens. Science 340: 701–706.
2. Ehrt S, Schnappinger D, Bekiranov S, Drenkow J, Shi S, et al. (2001) Reprogramming of the macrophage transcriptome in response to interferon-gamma and Mycobacterium tuberculosis: signaling roles of nitric oxide synthase-2 and phagocyte oxidase. J Exp Med 194: 1123–1140.
3. Rusinova I, Forster S, Yu S, Kannan A, Masse M, et al. (2013) Interferome v2.0: an updated database of annotated interferon-regulated genes. Nucleic Acids Res 41: D1040–1046.
4. Kim BH, Shenoy AR, Kumar P, Bradfield CJ, MacMicking JD (2012) IFN-inducible GTPases in host cell defense. Cell Host Microbe 12: 432–444.
5. Haller O, Staeheli P, Kochs G (2009) Protective role of interferon-induced Mx GTPases against influenza viruses. Rev Sci Tech 28: 219–231.
6. Goujon C, Moncorge O, Bauby H, Doyle T, Ward CC, et al. (2013) Human MX2 is an interferon-induced post-entry inhibitor of HIV-1 infection. Nature 502: 559–562.
7. Liu Z, Pan Q, Ding S, Qian J, Xu F, et al. (2013) The Interferon-Inducible MxB Protein Inhibits HIV-1 Infection. Cell Host Microbe 14: 398–410.
8. Bernstein-Hanley I, Coers J, Balsara ZR, Taylor GA, Starnbach MN, et al. (2006) The p47 GTPases Igtp and Irgb10 map to the Chlamydia trachomatis susceptibility locus Ctrq-3 and mediate cellular resistance in mice. Proc Natl Acad Sci U S A 103: 14092–14097.
9. Coers J, Bernstein-Hanley I, Grotsky D, Parvanova I, Howard JC, et al. (2008) Chlamydia muridarum evades growth restriction by the IFN-gamma-inducible host resistance factor Irgb10. J Immunol 180: 6237–6245.
10. Taylor GA, Collazo CM, Yap GS, Nguyen K, Gregorio TA, et al. (2000) Pathogen-specific loss of host resistance in mice lacking the IFN-gamma-inducible gene IGTP. Proc Natl Acad Sci U S A 97: 751–755.
11. Degrandi D, Konermann C, Beuter-Gunia C, Kresse A, Wurthner J, et al. (2007) Extensive characterization of IFN-induced GTPases mGBP1 to mGBP10 involved in host defense. J Immunol 179: 7729–7740.
12. Fentress SJ, Behnke MS, Dunay IR, Mashayekhi M, Rommereim LM, et al. (2010) Phosphorylation of immunity-related GTPases by a Toxoplasma gondii-secreted kinase promotes macrophage survival and virulence. Cell Host Microbe 8: 484–495.
13. Steinfeldt T, Konen-Waisman S, Tong L, Pawlowski N, Lamkemeyer T, et al. (2010) Phosphorylation of mouse immunity-related GTPase (IRG) resistance proteins is an evasion strategy for virulent Toxoplasma gondii. PLoS Biol 8: e1000576.
14. Bekpen C, Hunn JP, Rohde C, Parvanova I, Guethlein L, et al. (2005) The interferon-inducible p47 (IRG) GTPases in vertebrates: loss of the cell autonomous resistance mechanism in the human lineage. Genome Biol 6: R92.
15. Coers J (2013) Self and Non-self Discrimination of Intracellular Membranes by the Innate Immune System. PLoS Pathog 9: e1003538.
16. Howard JC, Hunn JP, Steinfeldt T (2011) The IRG protein-based resistance mechanism in mice and its relation to virulence in Toxoplasma gondii. Curr Opin Microbiol 14: 414–421.
17. Springer HM, Schramm M, Taylor GA, Howard JC (2013) Irgm1 (LRG-47), a regulator of cell-autonomous immunity, does not localize to mycobacterial or

listerial phagosomes in IFN-gamma-induced mouse cells. J Immunol 191: 1765–1774.
18. Haldar AK, Saka HA, Piro AS, Dunn JD, Henry SC, et al. (2013) IRG and GBP host resistance factors target aberrant, "non-self" vacuoles characterized by the missing of "self" IRGM proteins. PLoS Pathog 9: e1003414.
19. Hunn JP, Koenen-Waisman S, Papic N, Schroeder N, Pawlowski N, et al. (2008) Regulatory interactions between IRG resistance GTPases in the cellular response to Toxoplasma gondii. EMBO J 27: 2495–2509.
20. Papic N, Hunn JP, Pawlowski N, Zerrahn J, Howard JC (2008) Inactive and active states of the interferon-inducible resistance GTPase, Irga6, in vivo. J Biol Chem 283: 32143–32151.
21. Pawlowski N, Khaminets A, Hunn JP, Papic N, Schmidt A, et al. (2011) The activation mechanism of Irga6, an interferon-inducible GTPase contributing to mouse resistance against Toxoplasma gondii. BMC Biol 9: 7.
22. Al-Zeer MA, Al-Younes HM, Braun PR, Zerrahn J, Meyer TF (2009) IFN-gamma-inducible Irga6 mediates host resistance against Chlamydia trachomatis via autophagy. PLoS One 4: e4588.
23. Khaminets A, Hunn JP, Konen-Waisman S, Zhao YO, Preukschat D, et al. (2010) Coordinated loading of IRG resistance GTPases on to the Toxoplasma gondii parasitophorous vacuole. Cell Microbiol 12: 939–961.
24. Zhao Z, Fux B, Goodwin M, Dunay IR, Strong D, et al. (2008) Autophagosome-independent essential function for the autophagy protein Atg5 in cellular immunity to intracellular pathogens. Cell Host Microbe 4: 458–469.
25. Selleck EM, Fentress SJ, Beatty WL, Degrandi D, Pfeffer K, et al. (2013) Guanylate-binding protein 1 (Gbp1) contributes to cell-autonomous immunity against Toxoplasma gondii. PLoS Pathog 9: e1003320.
26. Tanida I (2011) Autophagy basics. Microbiol Immunol 55: 1–11.
27. Nishida Y, Arakawa S, Fujitani K, Yamaguchi H, Mizuta T, et al. (2009) Discovery of Atg5/Atg7-independent alternative macroautophagy. Nature 461: 654–658.
28. Sanjuan MA, Dillon CP, Tait SW, Moshiach S, Dorsey F, et al. (2007) Toll-like receptor signalling in macrophages links the autophagy pathway to phagocytosis. Nature 450: 1253–1257.
29. Hwang S, Maloney NS, Bruinsma MW, Goel G, Duan E, et al. (2012) Nondegradative role of Atg5-Atg12/Atg16L1 autophagy protein complex in antiviral activity of interferon gamma. Cell Host Microbe 11: 397–409.
30. Chang TK, Shravage BV, Hayes SD, Powers CM, Simin RT, et al. (2013) Uba1 functions in Atg7- and Atg3-independent autophagy. Nat Cell Biol 15: 1067–1078.
31. Kuma A, Hatano M, Matsui M, Yamamoto A, Nakaya H, et al. (2004) The role of autophagy during the early neonatal starvation period. Nature 432: 1032–1036.
32. Sou YS, Waguri S, Iwata J, Ueno T, Fujimura T, et al. (2008) The Atg8 conjugation system is indispensable for proper development of autophagic isolation membranes in mice. Mol Biol Cell 19: 4762–4775.
33. Yamamoto M, Okuyama M, Ma JS, Kimura T, Kamiyama N, et al. (2012) A Cluster of Interferon-gamma-Inducible p65 GTPases Plays a Critical Role in Host Defense against Toxoplasma gondii. Immunity.
34. Wang Y, Kahane S, Cutcliffe LT, Skilton RJ, Lambden PR, et al. (2011) Development of a transformation system for Chlamydia trachomatis: restoration of glycogen biosynthesis by acquisition of a plasmid shuttle vector. PLoS Pathog 7: e1002258.
35. Traver MK, Henry SC, Cantillana V, Oliver T, Hunn JP, et al. (2011) Immunity-related gtpase M (IRGM) proteins influence the localization of guanylate-binding protein 2 (GBP2) by modulating macroautophagy. J Biol Chem.
36. Scidmore MA, Hackstadt T (2001) Mammalian 14-3-3beta associates with the Chlamydia trachomatis inclusion membrane via its interaction with IncG. Mol Microbiol 39: 1638–1650.
37. Bernstein-Hanley I, Balsara ZR, Ulmer W, Coers J, Starnbach MN, et al. (2006) Genetic analysis of susceptibility to Chlamydia trachomatis in mouse. Genes Immun 7: 122–129.
38. Collazo CM, Yap GS, Sempowski GD, Lusby KC, Tessarollo L, et al. (2001) Inactivation of LRG-47 and IRG-47 reveals a family of interferon gamma-inducible genes with essential, pathogen-specific roles in resistance to infection. J Exp Med 194: 181–188.
39. Coers J, Gondek DC, Olive AJ, Rohlfing A, Taylor GA, et al. (2011) Compensatory T Cell Responses in IRG-Deficient Mice Prevent Sustained Chlamydia trachomatis Infections. PLoS Pathog 7: e1001346.
40. Henry SC, Daniell XG, Burroughs AR, Indaram M, Howell DN, et al. (2009) Balance of Irgm protein activities determines IFN-gamma-induced host defense. J Leukoc Biol 85: 877–885.
41. Degrandi D, Kravets E, Konermann C, Beuter-Gunia C, Klumpers V, et al. (2013) Murine guanylate binding protein 2 (mGBP2) controls Toxoplasma gondii replication. Proc Natl Acad Sci U S A 110: 294–299.
42. Kravets E, Degrandi D, Weidtkamp-Peters S, Ries B, Konermann C, et al. (2012) The GTPase activity of murine guanylate-binding protein 2 (mGBP2) controls the intracellular localization and recruitment to the parasitophorous vacuole of Toxoplasma gondii. J Biol Chem 287: 27452–27466.
43. Al-Zeer MA, Al-Younes HM, Lauster D, Abu Lubad M, Meyer TF (2013) Autophagy restricts Chlamydia trachomatis growth in human macrophages via IFNG-inducible guanylate binding proteins. Autophagy 9: 50–62.
44. Tietzel I, El-Haibi C, Carabeo RA (2009) Human guanylate binding proteins potentiate the anti-chlamydia effects of interferon-gamma. PLoS One 4: e6499.
45. Ling YM, Shaw MH, Ayala C, Coppens I, Taylor GA, et al. (2006) Vacuolar and plasma membrane stripping and autophagic elimination of Toxoplasma gondii in primed effector macrophages. J Exp Med 203: 2063–2071.
46. Martens S, Parvanova I, Zerrahn J, Griffiths G, Schell G, et al. (2005) Disruption of Toxoplasma gondii parasitophorous vacuoles by the mouse p47-resistance GTPases. PLoS Pathog 1: e24.
47. Virreira Winter S, Niedelman W, Jensen KD, Rosowski EE, Julien L, et al. (2011) Determinants of GBP recruitment to Toxoplasma gondii vacuoles and the parasitic factors that control it. PLoS One 6: e24434.
48. Slobodkin MR, Elazar Z (2013) The Atg8 family: multifunctional ubiquitin-like key regulators of autophagy. Essays Biochem 55: 51–64.
49. Dupont N, Jiang S, Pilli M, Ornatowski W, Bhattacharya D, et al. (2011) Autophagy-based unconventional secretory pathway for extracellular delivery of IL-1beta. EMBO J 30: 4701–4711.
50. Muller JM, Shorter J, Newman R, Deinhardt K, Sagiv Y, et al. (2002) Sequential SNARE disassembly and GATE-16-GOS-28 complex assembly mediated by distinct NSF activities drives Golgi membrane fusion. J Cell Biol 157: 1161–1173.
51. Sagiv Y, Legesse-Miller A, Porat A, Elazar Z (2000) GATE-16, a membrane transport modulator, interacts with NSF and the Golgi v-SNARE GOS-28. EMBO J 19: 1494–1504.

OPEN

Gene Therapy (2015), 1–9

www.nature.com/gt

ORIGINAL ARTICLE

# Preferable sites and orientations of transgene inserted in the adenovirus vector genome: The E3 site may be unfavorable for transgene position

M Suzuki, S Kondo, Z Pei[1], A Maekawa, I Saito and Y Kanegae

The adenovirus vector (AdV) can carry two transgenes in its genome, the therapeutic gene and a reporter gene, for example. The E3 insertion site has often been used for the expression of the second transgene. A transgene can be inserted at six different sites/orientations: E1, E3 and E4 sites, and right and left orientations. However, the best combination of the insertion sites and orientations as for the titers and the expression levels has not sufficiently been studied. We attempted to construct 18 AdVs producing GFP or LacZ gene driven by the EF1α promoter and Cre gene driven by the α-fetoprotein promoter. The AdV containing GFP gene at E3 in the rightward orientation (GFP-E3R) was not available. The LacZ-E3R AdV showed 20-fold lower titer and 50-fold lower level of fiber mRNA than the control E1L AdV. Notably, we found four aberrantly spliced mRNAs in the LacZ-E3L/R AdVs, probably explaining their very low titers. Although the transgene expression levels in the E4R AdVs were about threefold lower than those in the E1L AdVs, their titers are comparable with that of E1L AdVs. We concluded that E1L and E4R sites/orientations are preferable for expressing the main target gene and a second gene, respectively.

*Gene Therapy* advance online publication, 15 January 2015; doi:10.1038/gt.2014.124

## INTRODUCTION

First-generation (E1 deleted) adenovirus vectors (FG AdVs), which lack the E1 and E3 regions, are popularly used in basic studies to elucidate gene functions, and have been employed for gene therapy.[1–4] Because the DNA fragments of up to about 7 kilobases (kb) in total can be inserted into the AdV genome, the AdVs are frequently used to produce two proteins simultaneously from two independent transgenes expressing both the target gene and the reporter gene, for example. In the studies using the cultured cells and in the animal experiments, the GFP and luciferase are used as the reporters. Recently, positron emission tomography has clinically been used in patients for diagnoses and in experimental animal models. Therefore, the AdVs containing both the therapeutic gene and the positron emission tomography reporter gene would be valuable in the gene therapy fields, because the therapeutic effects, the vector duration and distribution can simultaneously be monitored.[5–8] Probably one would wish for high-titer AdVs with the highest expression for the therapeutic gene and with the second highest for the reporter gene not causing any trouble, if the insertion sites and orientations in the AdV genome can be chosen. However, the titers and the expression levels of the AdVs may considerably be influenced by the sites and orientations of the transgenes. Such information may be very valuable for construction of the best vector, especially in the vector containing both the therapeutic gene and the reporter gene.

The simultaneous expression of two genes could be achieved by inserting the two genes into the E1 site under the control of a single prompter using the internal ribosomal entry sites or using porcine teschovirus-1 2A.[9,10] In the former approach, the expression of the second gene might be influenced by the sequences between internal ribosomal entry sites and its initiation codon, and in the latter, the manipulation is necessary to remove the stop codon of the first gene and to adjust the frames of the two genes. When two genes driven by the independent promoters are inserted into the E1 site, they might interfere with each other. However, when two independent expression units are inserted in different sites in the AdV genome, no interference occurs. Moreover, the advantage of this approach is that the main target gene can easily be changed using the AdV cassette that already contains the reporter gene.

There are three insertion sites and two orientations: a transgene can be inserted into the AdV genome by substitution of the E1 or E3 gene and by simple insertion at a position upstream of the E4 gene. Therefore, there are six different possible sites/orientations for any given transgene. Moreover, not only the potent promoters such as EF1α but also tissue-specific promoters such as α-fetoprotein (AFP) can also be employed. Although the studies examining which sites/orientations are superior to others are practically important, they have been very limited[11,12] and systematic analyses have not been reported so far.

As it is known that the expression level of a transgene varies considerably depending on the site in the cell chromosome of the human genome, the phenomenon is called the 'position effect'.[13,14] Although CG-methylation in the cell chromosome is clearly one reason, it is not observed in the AdV genome. Therefore, it would be of interest to examine whether the 'position effect' might also be observed similarly in the AdV genome for the potent promoter and for the tissue-specific promoter.

Laboratory of Molecular Genetics, The Institute of Medical Science, The University of Tokyo, Minato-ku, Tokyo, Japan. Correspondence: Dr Y Kanegae, Laboratory of Molecular Genetics, The Institute of Medical Science, The University of Tokyo, 4-6-1 Shirokanedai, Minato-ku, 108-8639, Tokyo, Japan.
E-mail: kanegae@ims.u-tokyo.ac.jp
[1]Current address: CDM (Contract Development & Manufacturing) center, Takara Bio Inc., 3-4-1 Seta, Otsu, Shiga, Japan.
Received 15 August 2014; revised 5 November 2014; accepted 20 November 2014

FG AdVs retain almost all viral genes. They are normally not expressed in the target cells, because E1A protein, the essential transactivator for expression of all other viral genes, is not present. However, there is one report of splicing of aberrant mRNAs from the inserted foreign genes to a viral gene.[15] In this case, the aberrant mRNAs are transcribed by strong foreign promoters and produce transgene-viral gene fusion proteins, which elicit strong immune responses. However, it is not known whether the production of the aberrant gene product between the inserted transgene and viral gene is rare or not.

In this study, we examined the AdV titers and expression levels of an identical transgene inserted at the E1, E3 and E4 sites. We used three transgenes, namely, GFP, LacZ and Cre, and two promoters, namely, the potent EF1α promoter and the cancer-specific AFP promoter, and attempted to construct AdVs using all combinations, that is, 18 AdVs, and succeeded in constructing 17 of them. We found that insertion at the E1 and E4 sites yielded mostly high titers, whereas the one at the E3 yielded variable titers. Surprisingly, four aberrantly spliced mRNAs between the transgenes and viral genes were found in the vector obtained by insertion at the E3 site, which was probably the reason for the very low titers. As for the expression levels, clear differences were observed among the vectors obtained with insertion at the E1, E3 and E4 sites despite using the identical transgene, indicating that the position effect was certainly present for the AdV genome and that aberrant splicing may, at least in part, explain this effect. We also propose a strategy to avoid generation of the aberrantly spliced mRNAs.

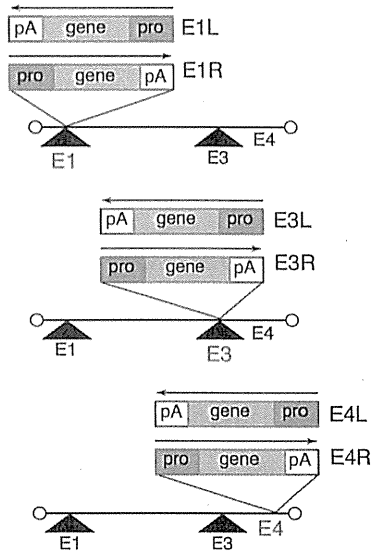


**Figure 1.** The FG AdV structures of six different site/orientations in all possible combinations. The box containing 'pro,' 'gene' and 'pA' represents the expression unit and the arrows show the orientation of transcription. 'pro,' EF1α and AFP promoter; gene, GFP, LacZ and Cre; pA, rabbit β-globin polyadenylation signal. For example, the vector containing the transgene at the E1 insertion site and in the left orientation is denoted as 'E1L.'

## RESULTS

### The vector titers were significantly influenced by the insertion sites and orientations of the transgene

We first examined whether the vector titers were influenced by the site/orientations of the transgenes containing a potent EF1α promoter. Towards this end, we attempted to construct six GFP-expressing (EF-GFP) and six LacZ-expressing (EF-LacZ) vectors in all possible combinations, that is, the E1, E3 and E4 insertion sites and the two orientations (Figure 1), and measured the vector titers (Figure 2a) (hereinafter, the vectors will be designated as per the following; the vectors containing the GFP gene and LacZ gene at the E1 insertion site and in the left orientation shall be denoted as G-E1L and Z-E1L vectors, respectively). Among the GFP-expressing vectors, high titers were obtained for G-E1L, G-E3L, G-E4L and G-E4R vectors (Figure 2a, bars 1, 3, 5 and 6), while the titer for the G-E1R vector was lower (bar 2). Notably, the G-E3R vector, that is, vector with the GFP transgene inserted in the E3 site in the rightward orientation, could not be obtained despite three independent attempts (bar 4, denote '×'). Therefore, although exactly the same EF1α-GFP expression unit was inserted in these vectors, the sites and orientations exerted considerable influence on the vector titers and even determined whether the vector was available or not. Similar results were obtained for vectors expressing LacZ: the titers of the Z-E1L, Z-E4L and Z-E4R vectors (bars 7, 11 and 12) were high, and that of the Z-E1R vector was also low (bar 8). However, the results of insertion at the E3 site differed for GFP and LacZ. The titer ratio of Z-E3L was significantly lower than that of G-E3L (compare bars 3 and 9, described later), and the Z-E3R vector was available, although its titer was extremely low (bar 10). Therefore, the GFP gene and LacZ gene themselves influenced the vector titers.

Then, we constructed six vectors containing the AFP promoter and Cre gene (AFP-Cre) and measured their titers (Figure 2b). Although these vectors contained the AFP promoter and Cre gene, this transgene unit served as a nonfunctional DNA, because the AFP promoter, which is hepatocarcinoma-cell-specific, is not active in the 293 cells. The titers of the all six vectors were very similar (Figure 2b). Thus, the site/orientation does not always influence the vector titers, and it appeared that there may be some specific reasons why the titers were low for vectors containing the EF1α promoter expressing the GFP and LacZ genes.

### Aberrant chimera mRNAs were produced in the vectors containing the expression unit at the E3 site

The E3 transgene is present within the large intron from the major late promoter (MLP) to the fiber gene (Figure 3a, except the first). We previously reported an aberrant splicing from a cryptic donor site present in the LacZ gene to the viral pIX acceptor site, which produces a LacZ-pIX fusion protein.[15] Therefore, we speculated that similar aberrant splicing might occur for the LacZ gene inserted at the E3 site.

Total RNA was prepared from the 293 cells infected with the E3R vector and reverse-transcribed to detect such aberrantly spliced mRNA spanning from the LacZ cryptic donor site to the possible fiber acceptor site, which is the only acceptor site present downstream of the LacZ donor site. In fact, we identified an aberrant mRNA spliced from this LacZ donor to the fiber acceptor (Figure 3a, second; Figure 3b, 0.7-kb band). The splicing donor site in the LacZ gene was identical to that of the reported LacZ gene inserted at E1 site to the viral pIX acceptor site, and the fiber acceptor site was the same as that normally spliced from the MLP donor site (Supplementary Table S1). This is quite abnormal because, in general, splicing occurs between only specific donor and acceptor sites, suggesting that an inserted transgene could disturb normal splicing.

We also examined whether any other aberrantly spliced mRNA upstream of the transgene was present or not. Surprisingly, we also detected an abnormal mRNA spliced from the donor site of the third exon of the viral MLP to the acceptor site of the second exon of the EF1α promoter (Figure 3a, third; Figure 3b, 1.2-kb band; the junction sequence is shown in Supplementary Table S1). These results mean that the normal splicing from the MLP donor to the fiber acceptor are doubly competed with aberrant splicing

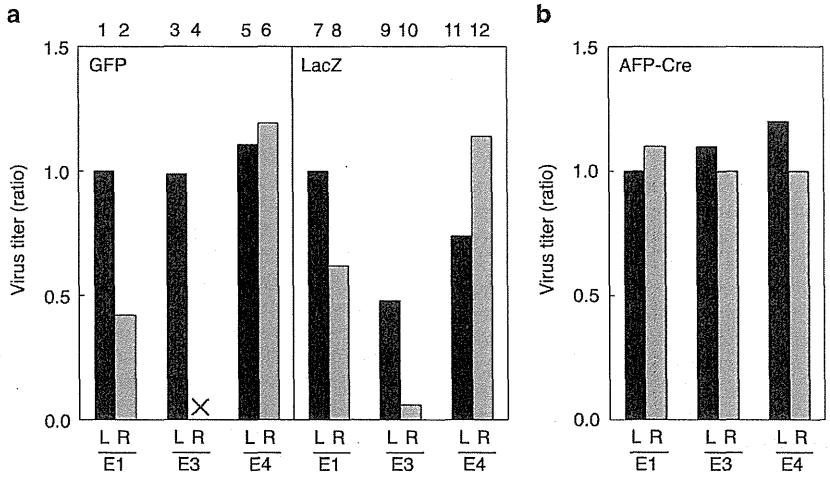


**Figure 2.** Titers of the virus vectors containing identical expression units. (**a**) Virus titers of the AdVs containing the EF1α promoter. The AdV genomes transduced into the HuH-7 cells were measured 3 days post infection. The virus titers were calculated relative to the copy numbers of the AdVs.[16] The titer of the E1L vector was set as 1; G-E1L, $8.3 \times 10^8$ relative virus titer (rVT)/ml, L-E1L, $5.0 \times 10^9$ rVT/ml. '×' indicates that G-E3R could not be obtained. (**b**) The titers of the virus vector containing Cre gene driven by the AFP promoter. E1L vector was used as the control. $^*P < 0.05$, $^{**}P < 0.01$.

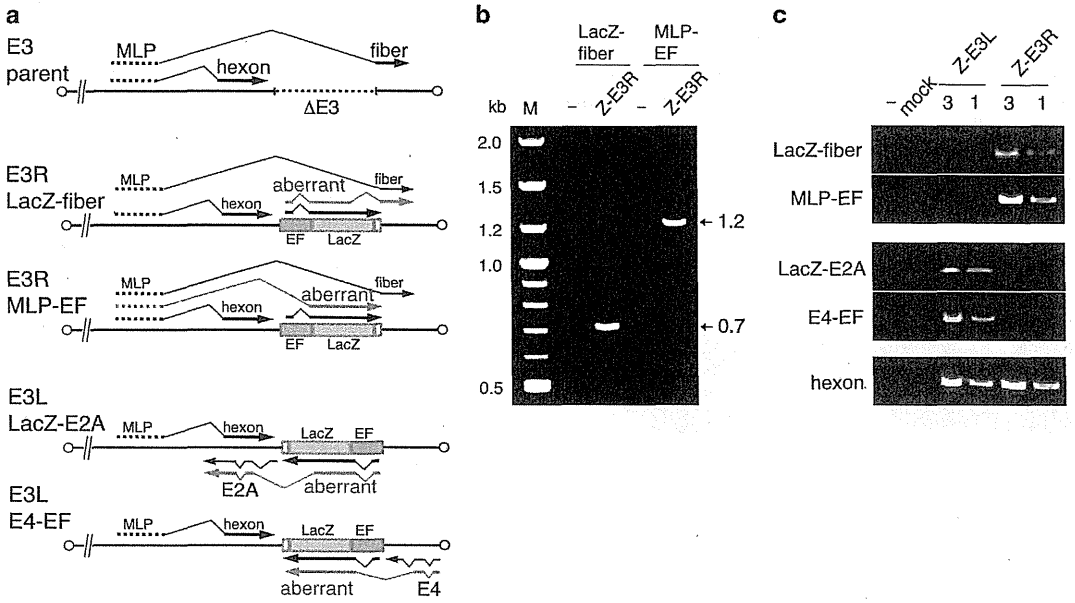


**Figure 3.** Structures of aberrant chimeric mRNAs. (**a**) Schematic representation of the aberrantly spliced mRNA and the expression unit in the E3 region. The LacZ expression units in the E3 region are shown. Aberrant mRNAs are shown in red. The bold lines and thin polygonal lines represent the exon and intron of the transcript, respectively. Arrow, orientation of the transcription; EF, EF1α promoter; LacZ, LacZ DNA. The 'parent' denotes the vectors before the insertion into the E3. 'LacZ-fiber,' 'MLP-EF,' 'LacZ-E2A' and 'E4-EF' indicate combinations of primers for detection of the chimeric mRNAs. (**b**) Detection of aberrant splicing by PCR. The 293 cells were infected with the Z-E3L and Z-E3R vectors, as indicated. The bands are generated from the chimera-specific mRNA between the viral gene and the inserted transgene. The primer sequences are shown in Supplementary Table S2. M, size maker; -, no DNA. (**c**) Specificity of the aberrant splicing. The 293 cells were infected with either Z-E3L or Z-E3R. The splicing from the MLP to hexon was used as the control. The bands of LacZ-fiber and MLP-EF in Z-E3R are the same as those described in (**b**) (0.7 and 1.2 kb, respectively). These bands were not detected in Z-E3L (lanes 3 and 1); threefold more DNA was loaded in lane 3 than in lane 1 to clearly show the semi-quantitative difference in the amount of cDNA. mock, mock infection of the 293 cells.

from the MLP donor to the EF1α acceptor and from LacZ donor to the fiber acceptor. We confirmed that these LacZ-fiber and MLP-EF aberrant mRNAs observed for the Z-E3R vector were not detected for the Z-E3L (Figure 3c, first and second rows).

We further examined whether such abnormal chimera mRNA was present for the Z-E3L vector of the opposite orientation. Actually, we detected two chimera mRNAs using the same PCR analysis; a viral E4 donor was spliced to the EF1α acceptor, and the

cryptic LacZ donor was spliced to a viral E2A acceptor (Figure 3a, fourth and fifth; Figure 3c, third and fourth rows. They were not detected for Z-E3R). The EF1α acceptor and LacZ donor were the same as those found in the E3L vector, and the sequences of the viral donor and the acceptor were identical to those found in the wild-type adenovirus, although the combinations were abnormal (Supplementary Table S1).

Then, we measured the amounts of fiber mRNA for the Z-E3R vector (very low titer) and compared them with those for the Z-E1L vector (high titer) and Z-E3L vector (medium titer) by conventional PCR and quantitative PCR (qPCR). These PCR and qPCR primers were designed to detect specifically the normal MLP-fiber mRNA, but not the aberrant mRNA, because they are prepared at the sequence junction: the forward and reverse primers are located in the MLP and fiber, respectively. The cDNAs from the 293 cells infected with Z-E1L, Z-E3L or Z-E3R were diluted from $10^0$ to $10^{-3}$ before PCR (shown as '0' to '−3' in Figure 4a) for semi-quantitative detection (Figure 4a). The level of normal fiber mRNA of Z-E3L (middle titer) was lower and that of Z-E3R (very low titer) was much lower than that of Z-E1L (high titer), that is, the fiber mRNA levels and titers were well correlated. Notably, the amount of fiber mRNA of the Z-E3R vector was only 2% of that for the Z-E1L vector (Figure 4b, E3R). This may probably explain why the titer of Z-E3R was very low.

### The expression of the E1 transgenes was higher than that of the E3 or E4 transgenes

The titers show amounts of infections virus particles produced by the vectors growing in the 293 cells, while expression levels are also important for the vector. The amounts of the produced gene products being influenced by the position of an identical expression unit on the cell chromosomes is referred to as the 'position effect' of gene expression.[13,14] To examine whether identical transgenes inserted into vector genomes are influenced or not by the 'position effect,' we infected the HuH-7 cells with the same numbers of active vector particles[16] expressing GFP under the control of the EF1α promoter at multiplicity of infection (MOI) 3 and 10 and measured the amounts of GFP mRNAs by qPCR (Figure 5a).

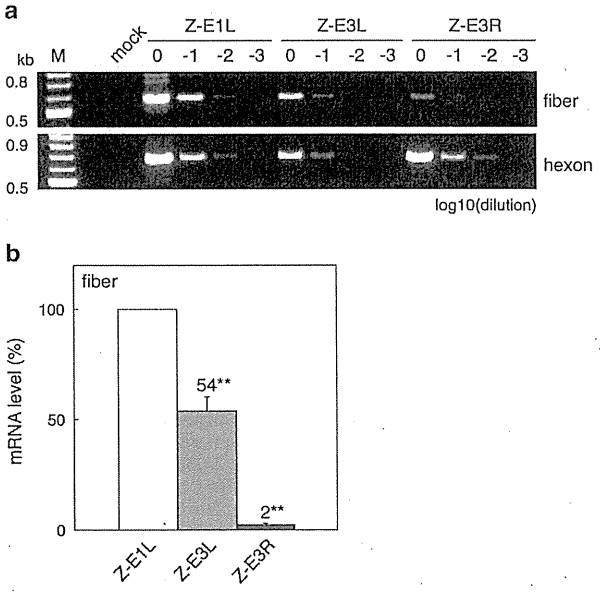


**Figure 4.** The relative levels of fiber mRNAs. The 293 cells were infected with the Z-E1L, Z-E3L and Z-E3R at MOI 5. (**a**) PCR detection of the fiber and hexon mRNAs. '0, -1, -2 and -3' mean '$10^0$, $10^{-1}$, $10^{-2}$ and $10^{-3}$ dilution of the cDNAs', respectively. M, size marker; mock, mock infection of 293 cells. (**b**) The quantities of the fiber and hexon mRNAs determined by qPCR. Amount of fiber mRNA relative to those of each hexon and Z-E1L fiber are regarded as 100%. $n=3$; means ± s.d. ** $P<0.01$.

E1L and E1R vectors expressed much more GFP mRNA than the other three vectors, that is, the E3L, E4L and E4R vectors, both at MOI 3 and MOI 10 (bars 2 and 3 to 4, 6 and 7; bars 8 and 9 to 10, 12 and 13). In regard to the expression levels of these vectors, the mRNA amounts of the E4 vectors were about one-third of those of the E1 vectors. Similar results were obtained for the vectors expressing LacZ: E1L/R vectors expressed much more LacZ mRNA than all the E3 and E4 vectors, both at MOI 3 and MOI 10 (Figure 5b, bars 2 and 3 to 4–7; bars 8 and 9 to 10–13). Therefore, similar effects were observed using two different genes. These results might suggest that the position effect observed here was not dependent on the inserted transgene. It should be noted that about as much as a 50-fold more virus stock solution of Z-E3R vector could be needed than that of the Z-E1L vector to obtain the same expression level, because the titer of Z-E3R vector was about one-tenth and the expression level obtained was about one-fifth when the same volume of the virus stock solution is used for infection (Figure 2a, bars 7 and 10; Figure 5b, bars 2–5 and 8–11). We also measured the expressed protein levels of GFP and LacZ using fluorometry and β-galactosidase assay, respectively (Figure 6a and b). The G-E1 vectors produced significantly more GFP than the G-E4 vectors (Figure 6a, bars 2 and 3 to 6 and 7; bars 8 and 9 to 12 and 13), although the G-E3L vector expressed a similar level to that of the G-E1 vectors (bars 4 and 10). Also, the Z-E1 vectors expressed more LacZ than the Z-E3 and Z-E4 vectors (Figure 6b, bars 2 and 3 to 4–7; bars 8 and 9 to 10–13). These results in respect of the protein level confirm the mRNA expression levels measured by qPCR shown in Figure 5a and b.

To examine whether the position effects may also be observed for a tissue-specific promoter and for genes other than GFP and LacZ, the HuH-7 cells were infected with the vector expressing Cre under the control of the AFP promoter and the Cre expression levels were measured. The AFP promoter is specifically active in the HuH-7 cells derived from hepatocarcinoma in contrast to the case in the 293 cells. Because tissue-specific promoters, including the AFP promoter, are generally weak, the expressed Cre mRNA level was too low to measure quantitatively. Therefore, we used the method of 'excisional expression,' where the Cre enzyme driven by the AFP promoter switched on the potent EF1α promoter and specifically enhanced the expression level of dsRed by about 50-fold[17] (the strategy is shown in Supplementary Figure S1). The results were again very similar to those obtained using the EF1α promoter (Figure 6a and b): the AFP-E3 and E4 vectors expressed only about a half to one-fifth of dsRed mRNA than the AFP-E1 vectors (Figure 5c, bars 3 and 4 to 5–8, 9 and 10 to 11–14). Therefore, although the vector titers obtained using the AFP promoter were not influenced by their insertion sites (Figure 2b), the position effects at the E1, E3 and E4 sites showed very similar patterns to those of the EF1α promoter. Altogether, the E3L/R and E4L/R vectors expressed about two to fivefold less transgene products than the E1L/R vectors, not only when the potent EF1α promoter was used, but also when the tissue-specific AFP promoter was used, suggesting there may be a mechanism common to these promoters.

To examine whether the position effect of expression observed in the HuH-7 cells may also be observed in other cells, the HeLa cells were infected with the GFP-expressing vectors at MOI 3 and at MOI 10 (Figure 7a and b). The G-E1L vector expressed a significantly greater amount of mRNA than the G-E3 and G-E4 vectors (Figure 7a, bars 2 to 4, 6 and 7; bars 8 to 10, 12 and 13). However, the mRNA level of the E1R vector was not significantly different from those of the E3 and E4 vectors, because the

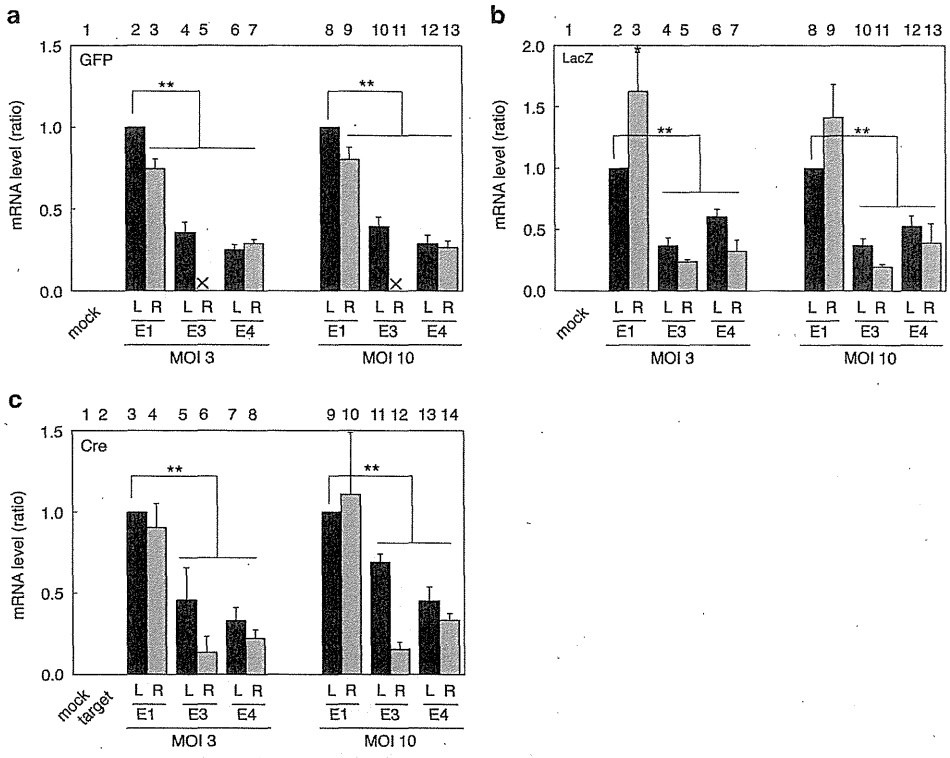


**Figure 5.** Expression levels of the transgene mRNA in the infected HuH-7 cells. The mRNA levels are shown relative to the mRNA level of the transgene in E1L-infected cells set as 1. (**a**) GFP mRNA levels. The cells were infected with the EF-GFP AdVs at the indicated MOIs. The GFP mRNA levels were quantified by qPCR, $n=3$. (**b**) LacZ mRNA levels. The cells were infected with the EF-LacZ AdVs. LacZ mRNA levels are shown in the same manner as that described in (**a**), $n=4$. (**c**) Cre mRNAs levels. The cells were co-infected with the AFP-Cre AdVs (switch vectors) and a target vector which expressed dsRed by Cre-mediated recombination (excisional expression). The dsRed mRNA levels were quantified in the same manner as that described in (**a**), $n=6$. Error bars indicate mean ± s.d; mock, HuH-7 cells without infection; target, HuH-7 cells infected with the target vector only; $^{*}P<0.05$, $^{**}P<0.01$. The other representations are the same as those in Figure 1.

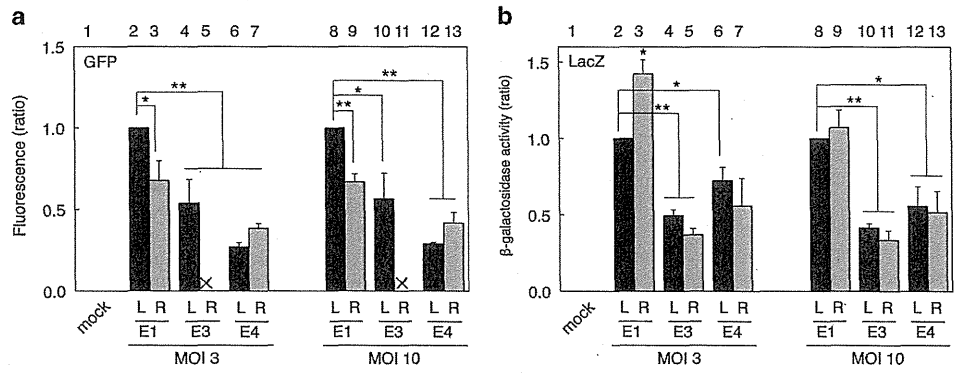


**Figure 6.** Protein expression levels in the infected HuH-7 cells. (**a**) Fluorescence of GFP. The cells were infected with the EF-GFP AdVs at the indicated MOIs. The fluorescence of GFP was quantified by Ascent fluorometry. The fluorescences are shown relative to the fluorescence level in E1L-infected cells set as 1, $n=4$. (**b**) Activities of β-galactosidase. The cells were infected with the EF-LacZ AdVs. β-galactosidase activities were evaluated by the β-gal assay, $n=3$. Error bars represent ± s.d.; mock, mock infection of HuH-7 cells; $^{*}P<0.05$, $^{**}P<0.01$. The other representations are the same as those in Figure 1.

expressed mRNA level of the E1R was lower than that of the E1L (bars 3 to 4, 6 and 7; bars 9 to 10, 12 and 13). Similar results were obtained using GFP fluorometry: the G-E1L vector exhibited significantly more fluorescence than the other G-E3 and G-E4 vectors (Figure 7b, bars 2 to 4, 6 and 7), whereas the E1R vector expression was not statistically significant (bars 3 to 4, 6 and 7). These results were confirmed by fluorescence microscopy (Supplementary Figure S2a). Moreover, the same results were obtained using the CV-1 cell line derived from monkey fibroblasts (Supplementary Figure S2b). Therefore, very similar position effect

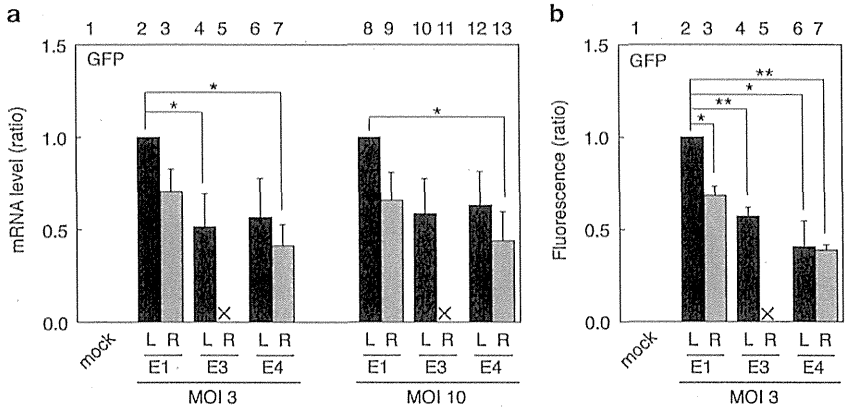


**Figure 7.** Expression levels of the transgene mRNA and protein in the infected HeLa cells. (**a**) GFP mRNA levels. The HeLa cells were infected with the EF-GFP AdVs at the indicated MOIs. The other representations are the same as those in Figure 4a, $n=3$. (**b**) Fluorescence of GFP. The HeLa cells were infected with EF-GFP AdVs at MOI 3. The other representations are the same as those in Figure 5a, $n=4$. Error bars indicate mean ± s.d.; mock, mock infection of HeLa cells; $^{*}P<0.05$, $^{**}P<0.01$.

among the E1, E3 and E4 insertion sites are obtained at least for the G-E1L vector.

## DISCUSSION

We demonstrated in this study that the inserted sites and orientations for a given transgene greatly influenced the vector titers and expression levels. Especially, when the transgene was inserted in E3R, the GFP-expressing vector could not be obtained and the LacZ-expressing vector titer was extremely low. Also, the titer of E3L AdV was lower than that of E1L AdV. Because the aberrantly spliced mRNAs from the transgenes to a viral gene have been reported for the E1R site/orientation[15] (described below), and similar aberrant splicing might have occurred for E4L site/orientation in the same mechanism. Therefore, considering the titers, aberrant splicing and expression levels, E1L and E4R sites/orientations were preferable for the main target gene and the second gene, respectively, in the simultaneous expression. As for the titer, the information might be useful not only for FG AdVs but also for the replication-competent AdVs containing E1A gene under the control of a cancer-specific promoter, because they both are prepared using the 293 cells.

We have demonstrated that the vectors containing transgene at E1L/R showed higher titers and expression levels than other vectors. E1L/R is the most frequently used, probably because the E1 site is required or convenient for the major methods of AdV construction which are now commonly used.[18–20] For example, for the method established by the Graham's group, the use of the E1 site is essential because it exploits the viral packaging sequences partially overlapping with the E1 region. Consequently, we think that the E1 site, found to be the best in this work, might have been chosen in the currently popular methods. However, there seems to be one concern with E1R: aberrant splicing has been reported to occur to viral pIX gene from the cryptic donors present not only in the LacZ gene but also in the herpes thymidine-kinase (TK) gene, which is used for positron emission tomography as a reporter gene and for suicide gene therapy. Consequently, TK-pIX and LacZ-pIX fusion proteins were produced, and the pIX protein evokes strong immune responses.[15] For this reason, we always adopt the leftward orientation for the E1 site.

Currently, in the simultaneous expression of the target gene and the reporter gene, the E3 sites are mostly employed for the reporter gene.[21–25] However, as described here, when the LacZ-expressing transgene driven by the EF1α promoter was inserted at E3R, the vector titer and expression level were very low, probably because of the aberrant splicing, and the G-E3R AdV could not be obtained. In our experiences, the E3R AdV containing GFP gene driven by SRα promoter[26] could also not be obtained. In contrast, however, the E3R AdV containing GFP driven by CMV promoter could be obtained. The reason of such difference is unclear, but it might be related to the fact that both EF1α and SRα promoters contain the splicing unit including the splicing acceptor site in their promoters, which might produce the aberrant mRNA spliced from the MLP donor, but the CMV promoter contain no splicing unit. Because aberrant splicing was detected even at E3L, both E3R and E3L were problematic and to be avoided, if possible.

The E4 site has not frequently been used.[17,19,27–29] The E4 insertion position, *Sna*BI site, is located 162 nucleotides (nt) from the right end of the AdV genome. Vectors containing a transgene at the E4 site showed high titers, although their expression levels were lower than those of the E1 vectors. The titers and expression levels do not significantly differ between E4L and E4R vectors. However, the E4L might produce aberrantly spliced mRNAs as observed for the E3L/R. The E4R site/orientation was successfully used as the position of the second transgene[17] where Cre was expressed under the control of the AFP promoter. The expressed Cre turned on the potent promoter present at the E1L and the high-level expression of the target gene was obtained, while maintaining strict sepecificity. Interestingly, it was also recently reported that the E4L, not the E4R, is better than the E1 site for short hairpin RNA expression.[27] The difference may be related to the use of the RNA polymerase III promoter for the short hairpin RNA production, whereas the polymerase II promoter is used for the protein production. If so, the E4L may be advantageous not only for the production of short hairpin RNA, but also of guide RNAs used for the CRISPR/Cas9 system.[30,31] The reported results might not contradict with the results described here, because the RNA polymerase III expression is not involved with splicing.

Altogether, therefore, the E1L and E4R sites/orientations appear to be the best for use in AdVs for the simultaneous expression of the target gene and reporter gene, respectively. Importantly, the occurrence of aberrant splicing sometimes yields a viral-transgene fusion protein, which may induce strong immune responses caused by the viral encoding region.[15] The probability is one-third to coincide the coding frame of the transgene with that of the viral gene. The coding regions of the four aberrant mRNAs described in this report were, by chance, connected out-of-frame, yielding no transgene-fusion protein, but only a truncated LacZ protein composed of several amino acids. However, in a previous study,[15] LacZ-pIX and TK-pIX fusion proteins were produced under the control of potent promoters. Thus, the production of such fusion proteins by aberrant splicing is not a rare event.

In general, use of the same promoter may cause troubles by the homologous recombination in the simultaneous recombination. We have experienced that, when the identical promoters in the E1L and E4R sites/orientations were applied, a rearrangement through the homologous recombination occurred, whereas the AdVs in the E1L and E4L was stable. Therefore, use of different promoters would be preferable.

The harmful aberrant splicing can be avoided using the technique described herein. The aberrant splicing can be identified by PCR analysis as reported here. The preferred sequences of the splicing donor site are AGGT/AAGT (slash denotes the exon-intron junction), where the underlined GT dinucleotides are definitely required for splicing. Nucleotide mutations of these sequences, especially the GT nucleotides, can be introduced without changing the amino acid encoded by the therapeutic gene, and successful disruption of the aberrant splicing can be easily confirmed by a subsequent PCR using the same primer set. As an example, the change from T to C, G or T (Gly) in the aberrant splicing present in the TK gene removes the splicing while keeping the amino acid sequence intact, and this mutated TK gene is expected to be safer than the original TK gene for suicide gene therapy and for positron emission tomography analyses using TK gene as a reporter.

The results described here demonstrated that position effects were evident for the expression of transgenes present on the AdV genome. The mechanisms of the position effect in the AdV genome are unknown. We think that viral enhancers, silencers or other *cis*-acting sequences near to the foreign transgene promoter might influence its expression. It might be related to the fact that similar results were obtained for a strong EF1α promoter and a cancer-specific AFP promoter. In contrast to the expression levels, the vector titers were probably not influenced by the position of the transgene, because similar and high titers were obtained using a tissue-specific promoter, which does not produce the transgene mRNA in the 293 cells (Figure 2b). The results might suggest that the vector titers were mainly influenced by the combination of a strong promoter and aberrant splicing between the transgene and viral genes (Figure 2a). These results are probably valuable for efficient and safe gene therapy using FG AdVs.

In this work, the range of the E3 deletion is between two *Xba*I sites in the E3 region (nt position 28,592–30,470). Because the lengths of the E3 deletions are slightly different among the commercially available AdV construction kits, the differences might influence the results obtained here. We surmise that these differences might not influence the conclusion described here as far as the same transgene is used, because the same splicing event is essentially expected to occur by the same mechanism. However, the possibility cannot be ruled out.

The cassette plasmids (also used as cosmids) are available on request in a collaboration basis, which bear the full-length AdV genome containing the unique *Swa*I site at the E1 site and the unique *Cla*I site at the E4 site (pAxw4cit2) and that inversely containing the *Cla*I site at the E1 site and *Swa*I at the E4 site (pAxc4wit2). The method to insert a transgene into these sites is described in the Materials and Methods section.

## MATERIALS AND METHODS

### Cells and virus titration

Human 293,[32] HeLa and HuH-7 cell lines are derived from the human embryonic kidney, human cervical carcinoma and human hepatocellular carcinoma, respectively. The CV-1 cell line is derived from African green monkey kidney. The cells were cultured in Dulbecco's Modified Eagles Medium supplemented with 10% fetal calf serum. The 293 cells constitutively express adenoviral E1 genes and support the replication of E1-substituted AdVs. After infection with AdVs, the cells were maintained in Dulbecco's Modified Eagles Medium supplemented with 5% fetal calf serum without geneticin. FG AdVs were titrated using the method described by Pei *et al.*[16] Briefly, the copy numbers of a viral genome that was successfully transduced into the infected target cells were measured by real-time PCR (relative virus titer). HuH-7 cells were used as the target cells. The titer of the standard virus was determined using the copy number of serially diluted plasmid DNA. When FG AdVs are used, the relative virus titer (copies per ml) normally corresponds to about one-fifth of the Tissue Culture Infectious Dose 50 titer, when the gene product is not deleterious; the probable reason for this difference is that the transduction efficiency of the 293 cells is exceptionally high as compared with that of the other cells. The sequences of the TaqMan probes for the titration are derived from adenovirus-5 (Ad5) pIX gene: forward primer, 5′-TGTG ATGGGCTCCAGCATT-3′; probe, 5′-ATGGTCGCCCCGTCCTGCC-3′; reverse primer, 5′-TCGTAGGTCAAGGTAGTAGAGTTTGC-3′.

### Vector construction

All the AdVs described here were constructed using the cosmid cassette pAxcwit2 containing the full-length AdV genome.[19,33] The GFP/LacZ-expression unit were under the control of the EF1α promoter[34] and the Cre-expression unit was driven by the AFP promoter; the AFP promoter used here was the (AB) 2S6 AFP promoter.[35] All the expression units were inserted into the *Swa*I cloning site at the E1 substitution region as E1L or R vectors. All the E3L and E3R vectors possessed the same expression units at the *Xba*I site in the E3 region of pAxcwit2; the *Xba*I site is originally generated by deletion between the two *Xba*I sites in the Ad5 genome (nt position 28,592-30,470). The E4 cloning site represented by the *Sna*BI site (nt position 35770) located in the E4 region at 165-nt downstream from the right end of the Ad5 genome.[17]

### Conventional PCR

The PCR experiments were essentially performed by the standard method.[36] Typically, the 293 cells in the 6-well plate were infected at MOI 5 and 16 h post infection, total RNAs were prepared and reverse-transcribed using oligo(dT) primer; the resultant cDNAs were amplified by PCR with Tks Gflex DNA polymerase (Takara Bio, Shiga, Japan) and a PCR system (ProFlex PCR system, Applied Biosystems, Foster City, CA, USA). The PCR cycling conditions were in accordance with the manufacturer's protocol (Takara Bio): 94 °C for 1 min, followed by 30 cycles at 98 °C for 10 s, 60 °C for 15 s, and 68 °C for 30 s. The primer sets are described in Supplementary Table S2. The PCR products containing each splice junction were subjected to agarose gel electrophoresis.

### Quantitative real-time PCR

The sequences of the GFP primers and the dsRed primers have been described previously.[17,37] The sequences of the LacZ primers were as follows: forward primer, 5′-ATCAGGATATGTGGCGGATGA-3′; probe, 5′-CGG CATTTTCCGTGACGTCT-3′; reverse primer, 5′-TGATTTGTGTAGTCGGTTTA TGCA-3′. The primer sequences of the normal splicing junctions of MLP-fiber and MLP-hexon were as follows: for MLP-fiber detection forward primer in MLP third exon, 5′-AAAGGCGTCTAACCAGTCACAGT-3′; probe in the fiber gene, 5′-AGCGCGAAGACCGTCTGAAGATACC-3′; reverse in the fiber gene, 5′-CCGCTTTCCGTGTCATATGG-3′; and for MLP-hexon detection forward primer in MLP third exon, 5′-TCTAACCAGTCACAGTCGCAAGA-3′; probe in the hexon gene, 5′-CGCGCCCGCTTTCCAAGATG-3′; reverse in the hexon gene, 5′-CACTGCGGCATCATCGAA-3′.

The mRNA levels were calculated as described by Maekawa *et al.*[37] Briefly, the total RNA of the infected cells was extracted, and the amounts of the expressed target RNAs and 18S-rRNA (correction standard) were quantified using reverse transcription (TaqMan Reverse Transcription Reagents, Roche, Basel, Switzerland) and real-time PCR (Applied Biosystems Prism 7000); the ratio of the target RNA to 18S-rRNA was then calculated. To quantify the AdV genome, the infected total cell DNA was prepared from the cells using a previously described method[29,38] or a DNA preparation kit (Macherey-Nagel, through Takara Bio). Quantitative PCR was performed to detect the AdV genome using a probe for the pIX gene, as described above.[17] The amount of chromosomal DNA was simultaneously measured to correct the Ct values of the viral genome per cell, and the corrected Ct is shown throughout. The probes were derived from the sequence of the human β-actin gene for the HeLa and HuH7 cell lines. The qPCR reaction was performed using the following cycling conditions according to the manufacturer's protocol (Applied BioSystems): 50 °C for 2 min and 95 °C for 10 min, followed by 40 cycles at 95 °C for 15 s and 60 °C for 1 min.

### Measurement of the expressed GFP and LacZ

The HuH-7, HeLa and CV1 cells were infected at MOI 3 or MOI 10 of each vector in a 24-well plate in triplicated experiments. Three days after the infection, the infected cells were washed twice with phosphate-buffered saline.The cells in the three wells were then fixed with 4% paraformaldehyde to quantify the GFP fluorescence using Labsystems Fluoroskan Ascent FL (GMI, Ramsey, MN, USA) or by fluorescence microscopy. The cells infected with the LacZ vectors were harvested for the quantification of β-galactosidase (β-gal) (β-gal assay kit, Invitrogen, Carlsbad, CA, USA). To quantify the β-gal activity, the infected cells were disrupted by sonication and the lysate was subjected to a color reaction assay using o-Nitrophenyl β-D-galactopyranoside. The stained color standard was determined using 5-bromo-4-chloro-3-indolyl-β-D-galactopyranoside (X-gal).

### Insertion of a transgene into the cassette plasmid (cosmid) containing both the E1 and E4 sites

The method of inserting a given transgene into the *Swa*I site of pAxw4cit2 and pAxc4wit2 is followed by the protocol of Takara Bio (Adenovirus Dual Expression Kit). Briefly, the plasmid containing the transgene DNA fragment is treated with the appropriate restriction enzymes and treated with the DNA polymerase I Klenow fragment, followed by agarose gel electrophoresis. The isolated transgene fragment of about 50 ng is ligated with 1–2 μg of the cassette cosmid at a volume of 15 μl at 15 °C for overnight. The ligated DNA is cleaved with *Swa*I to remove the self-ligated parent plasmid, and then transformation or lambda *in vitro* packaging is performed. The latter method is highly efficient and removes the deleted plasmids smaller than 38 kb. To insert a given transgene DNA to the *Cla*I site, the DNA fragment is treated with the Klenow polymerase and ligated with a DNA linker of *Bsp*T104I (Takara Bio, reaction temperature is 37 °C) or *Bst*BI (New England Biolabs, Ipswich, MA, USA, 65 °C), 5′-GGTTCGAACC-3′ (the underline shows the recognition sequences), for example, and digested with either enzyme. Because the termini produced with this enzyme can be ligated with *Cla*I-cleaved DNA and the ligated DNA cannot be cleaved with either enzyme. Therefore, after ligation of the transgene and *Cla*I-cleaved cassette, the self-ligated parent plasmid can be removed by *Cla*I digestion. Alternatively, both *Swa*I and *Cla*I sites can be converted to I-*Ceu*I, I-*Sse*I or both by insertion of the cleavage-site oligonucleotides.

## CONFLICT OF INTEREST

The authors declare no conflict of interest.

## ACKNOWLEDGEMENTS

We thank N Goda for research assistance and Ms T Shino for her secretarial assistance. This study was supported in part by Grants-in-Aids from the Ministry of Education, Culture, Sports, Science and Technology to YK and SK; The Program for Intractable Disease Research utilizing Disease-specific iPS Cells from JST to YK; a grant for Practical Research on Hepatitis B (009) from the Ministry of Health, Labour and Welfare of Japan to IS.

## REFERENCES

1 Crystal RG. Adenovirus: the first effective in vivo gene delivery vector. *Hum Gene Ther* 2014; **25**: 3–11.
2 Watanabe M, Nasu Y, Kumon H. Adenovirus-mediated REIC/Dkk-3 gene therapy: Development of an autologous cancer vaccination therapy (Review). *Oncol Lett* 2014; **7**: 595–601.
3 Wold WS, Toth K. Adenovirus vectors for gene therapy, vaccination and cancer gene therapy. *Curr Gene Ther* 2013; **13**: 421–433.
4 Danthinne X, Imperiale MJ. Production of first generation adenovirus vectors: a review. *Gene Ther* 2000; **7**: 1707–1714.
5 Gil JS, Machado HB, Campbell DO, McCracken M, Radu C, Witte ON *et al.* Application of a rapid, simple, and accurate adenovirus-based method to compare PET reporter gene/PET reporter probe systems. *Mol Imaging Biol* 2013; **15**: 273–281.
6 Qin C, Lan X, He J, Xia X, Tian Y, Pei Z *et al.* An in vitro and in vivo evaluation of a reporter gene/probe system hERL/(18)F-FES. *PloS One* 2013; **8**: e61911.
7 Zhang G, Lan X, Yen TC, Chen Q, Pei Z, Qin C *et al.* Therapeutic gene expression in transduced mesenchymal stem cells can be monitored using a reporter gene. *Nucl Med Biol* 2012; **39**: 1243–1250.
8 Gambhir SS, Barrio JR, Phelps ME, Iyer M, Namavari M, Satyamurthy N *et al.* Imaging adenoviral-directed reporter gene expression in living animals with positron emission tomography. *Proc Natl Acad Sci USA* 1999; **96**: 2333–2338.
9 Chan HY, V S, Xing X, Kraus P, Yap SP, Ng P *et al.* Comparison of IRES and F2A-based locus-specific multicistronic expression in stable mouse lines. *Plos One* 2011; **6**: e28885.
10 Kim JH, Lee SR, Li LH, Park HJ, Park JH, Lee KY *et al.* High cleavage efficiency of a 2A peptide derived from porcine teschovirus-1 in human cell lines, zebrafish and mice. *Plos One* 2011; **6**: e18556.
11 Small JC, Kurupati RK, Zhou X, Bian A, Chi E, Li Y *et al.* Construction and characterization of E1- and E3-deleted adenovirus vectors expressing two antigens from two separate expression cassettes. *Hum Gene Ther* 2014; **25**: 328–338.
12 Pham L, Nakamura T, Gabriela Rosales A, Carlson SK, Bailey KR, Peng KW *et al.* Concordant activity of transgene expression cassettes inserted into E1, E3 and E4 cloning sites in the adenovirus genome. *J Gene Med* 2009; **11**: 197–206.
13 Yankulov K. Dynamics and stability: epigenetic conversions in position effect variegation. *Biochem Cell Biol* 2013; **91**: 6–13.
14 Wilson C, Bellen HJ, Gehring WJ. Position effects on eukaryotic gene expression. *Annu Rev Cell Biol* 1990; **6**: 679–714.
15 Nakai M, Komiya K, Murata M, Kimura T, Kanaoka M, Kanegae Y *et al.* Expression of pIX gene induced by transgene promoter: possible cause of host immune response in first-generation adenoviral vectors. *Hum Gene Ther* 2007; **18**: 925–936.
16 Pei Z, Kondo S, Kanegae Y, Saito I. Copy number of adenoviral vector genome transduced into target cells can be measured using quantitative PCR: Application to vector titration. *Biochem Biophys Res Commun* 2012; **417**: 945–950.
17 Kanegae Y, Terashima M, Kondo S, Fukuda H, Maekawa A, Pei Z *et al.* High-level expression by tissue/cancer-specific promoter with strict specificity using a single-adenoviral vector. *Nucleic Acids Res* 2011; **39**: e7.
18 Bett AJ, Haddara W, Prevec L, Graham FL. An efficient and flexible system for construction of adenovirus vectors with insertions or deletions in early regions 1 and 3. *Proc Natl Acad Sci USA* 1994; **91**: 8802–8806.
19 Miyake S, Makimura M, Kanegae Y, Harada S, Sato Y, Takamori K *et al.* Efficient generation of recombinant adenoviruses using adenovirus DNA-terminal protein complex and a cosmid bearing the full-length virus genome. *Proc Natl Acad Sci USA* 1996; **93**: 1320–1324.
20 Mizuguchi H, Kay MA. Efficient construction of a recombinant adenovirus vector by an improved in vitro ligation method. *Hum Gene Ther* 1998; **9**: 2577–2583.
21 Shin SP, Seo HH, Shin JH, Park HB, Lim DP, Eom HS *et al.* Adenovirus Expressing Both Thymidine Kinase and Soluble PD1 Enhances Antitumor Immunity by Strengthening CD8 T-cell Response. *Mol Ther* 2013; **21**: 688–695.
22 Suzuki T, Sasaki T, Yano K, Sakurai F, Kawabata K, Kondoh M *et al.* Development of a recombinant adenovirus vector production system free of replication-competent adenovirus by utilizing a packaging size limit of the viral genome. *Virus Res* 2011; **158**: 154–160.
23 Trujillo MA, Oneal MJ, McDonough S, Qin R, Morris JC. A probasin promoter, conditionallfor exampley replicating adenovirus that expresses the sodium iodide symporter (NIS) for radiovirotherapy of prostate cancer. *Gene Ther* 2010; **17**: 1325–1332.
24 Mailly L, Boulade-Ladame C, Orfanoudakis G, Deryckere F. A novel adenovirus vector for easy cloning in the E3 region downstream of the CMV promoter. *Virol J* 2008; **5**: 73.
25 Mizuguchi H, Kay MA, Hayakawa T. In vitro ligation-based cloning of foreign DNAs into the E3 and E1 deletion regions for generation of recombinant adenovirus vectors. *Biotechniques* 2001; **30**: 1112–1114; 1116.
26 Takebe Y, Seiki M, Fujisawa J, Hoy P, Yokota K, Arai K *et al.* SR alpha promoter: an efficient and versatile mammalian cDNA expression system composed of the simian virus 40 early promoter and the R-U5 segment of human T-cell leukemia virus type 1 long terminal repeat. *Mol Cellular Biol* 1988; **8**: 466–472.
27 Pei Z, Shi G, Kondo S, Ito M, Maekawa A, Suzuki M *et al.* Adenovirus vectors lacking virus-associated RNA expression enhance shRNA activity to suppress hepatitis C virus replication. *Sci Rep* 2013; **3**: 3575.
28 Mizuguchi H, Xu ZL, Sakurai F, Mayumi T, Hayakawa T. Tight positive regulation of transgene expression by a single adenovirus vector containing the rtTA and tTS expression cassettes in separate genome regions. *Hum Gene Ther* 2003; **14**: 1265–1277.
29 Saito I, Oya Y, Yamamoto K, Yuasa T, Shimojo H. Construction of nondefective adenovirus type 5 bearing a 2.8-kilobase hepatitis B virus DNA near the right end of its genome. *J Virol* 1985; **54**: 711–719.
30 Cong L, Ran FA, Cox D, Lin SL, Barretto R, Habib N *et al.* Multiplex genome engineering using CRISPR/Cas systems. *Science* 2013; **339**: 819–823.
31 Mali P, Yang LH, Esvelt KM, Aach J, Guell M, DiCarlo JE *et al.* RNA-guided human genome engineering via Cas9. *Science* 2013; **339**: 823–826.

32 Graham FL, Smiley J, Russell WC, Nairn R. Characteristics of a human cell line transformed by DNA from human adenovirus type 5. *J Gen Virol* 1977; **36**: 59–74.

33 Fukuda H, Terashima M, Koshikawa M, Kanegae Y, Saito I. Possible mechanism of adenovirus generation from a cloned viral genome tagged with nucleotides at its ends. *Microbiol Immunol* 2006; **50**: 643–654.

34 Kim DW, Uetsuki T, Kaziro Y, Yamaguchi N, Sugano S. Use of the human elongation factor-1-alpha promoter as a versatile and efficient expression system. *Gene* 1990; **91**: 217–223.

35 Sato Y, Tanaka K, Lee G, Kanegae Y, Sakai Y, Kaneko S *et al.* Enhanced and specific gene expression via tissue-specific production of Cre recombinase using adenovirus vector. *Biochem Biophys Res Commun* 1998; **244**: 455–462.

36 Sambrook J, Russell DW. *Molecular Cloning: a laboratory manual*, 3rd edn. Cold Spring Harbor Laboratory Press: Cold Spring Harbor, New York, 2001.

37 Maekawa A, Pei Z, Suzuki M, Fukuda H, Ono Y, Kondo S *et al.* Efficient production of adenovirus vector lacking genes of virus-associated RNAs that disturb cellular RNAi machinery. *Sci Rep* 2013; **3**: 1136.

38 Nakano M, Odaka K, Takahashi Y, Ishimura M, Saito I, Kanegae Y. Production of viral vectors using recombinase-mediated cassette exchange. *Nucleic Acids Res* 2005; **33**: e76.



Supplementary Information accompanies this paper on Gene Therapy website (http://www.nature.com/gt)

OPEN ACCESS Freely available online

PLOS ONE

# Adenovirus-Encoding Virus-Associated RNAs Suppress HDGF Gene Expression to Support Efficient Viral Replication

**Saki Kondo[1], Kenji Yoshida[2], Mariko Suzuki[1], Izumu Saito[1], Yumi Kanegae[1]***

**1** Laboratory of Molecular Genetics, Institute of Medical Science, University of Tokyo, Shirokanedai, Minato-ku, Tokyo, Japan, **2** Regenerative and Cellular Medicine Office, Sumitomo Dainippon Pharma Co., Ltd., Minatojima Minamimachi, Chuo-ku, Kobe, Japan

## Abstract

Non-coding small RNAs are involved in many physiological responses including viral life cycles. Adenovirus-encoding small RNAs, known as virus-associated RNAs (VA RNAs), are transcribed throughout the replication process in the host cells, and their transcript levels depend on the copy numbers of the viral genome. Therefore, VA RNAs are abundant in infected cells after genome replication, i.e. during the late phase of viral infection. Their function during the late phase is the inhibition of interferon-inducible protein kinase R (PKR) activity to prevent antiviral responses; recently, mivaRNAs, the microRNAs processed from VA RNAs, have been reported to inhibit cellular gene expression. Although VA RNA transcription starts during the early phase, little is known about its function. The reason may be because much smaller amount of VA RNAs are transcribed during the early phase than the late phase. In this study, we applied replication-deficient adenovirus vectors (AdVs) and novel AdVs lacking VA RNA genes to analyze the expression changes in cellular genes mediated by VA RNAs using microarray analysis. AdVs are suitable to examine the function of VA RNAs during the early phase, since they constitutively express VA RNAs but do not replicate except in 293 cells. We found that the expression level of hepatoma-derived growth factor (HDGF) significantly decreased in response to the VA RNAs under replication-deficient condition, and this suppression was also observed during the early phase under replication-competent conditions. The suppression was independent of mivaRNA-induced downregulation, suggesting that the function of VA RNAs during the early phase differs from that during the late phase. Notably, overexpression of HDGF inhibited AdV growth. This is the first report to show the function, in part, of VA RNAs during the early phase that may be contribute to efficient viral growth.

**Citation:** Kondo S, Yoshida K, Suzuki M, Saito I, Kanegae Y (2014) Adenovirus-Encoding Virus-Associated RNAs Suppress HDGF Gene Expression to Support Efficient Viral Replication. PLoS ONE 9(10): e108627. doi:10.1371/journal.pone.0108627

**Editor:** Motoyuki Otsuka, The University of Tokyo, Japan

**Received** July 29, 2014; **Accepted** September 2, 2014; **Published** October 2, 2014



**Data Availability:** The authors confirm that all data underlying the findings are fully available without restriction. All relevant data except for the microarray data are within the paper and its Supporting Information files. All the data acquired by the microarray analysis were deposited in the NCBI Gene Expression Omnibus (NO. GSE58605).

**Funding:** This work was supported in part by Grants-in-Aid from the Ministry of Education, Culture, Sports, Science and Technology (http://www.jsps.go.jp/english/index.html) to S.K. and Y.K. and the Ministry of Health, Labour and Welfare (http://www.mhlw.go.jp/english/index.html) for Research on the Innovative Development and the Practical Application of New Drugs for Hepatitis B to I.S. This work was supported in part by the Program for Intractable Disease Research utilizing Disease-specific iPS Cells from JST to Y.K. The funders had no role in study design, data collection and analysis, decision to publish, or preparation of the manuscript.

**Competing Interests:** The authors of this manuscript have the following competing interests: K. Yoshida is employed by Dainippon Sumitomo Pharma Co., Ltd. This does not alter the authors' adherence to PLOS ONE policies on sharing data and materials.

* Email: kanegae@ims.u-tokyo.ac.jp

## Introduction

It has become increasingly clear over the past decade that non-coding small RNAs play roles in viral life cycles at various ways [1–3]. Hepatitis C virus (HCV) is known to utilize host microRNA miR122, which is specifically expressed and highly abundant in the human liver, to support its efficient replication through its direct attachment to the HCV 5′ non-translation region; thus, miR122 is regarded as a therapeutic target for antiviral intervention [4–6]. Moreover, more than two hundred small RNAs derived from viruses have been identified. For example, Epstein-Barr virus (EBV) encodes two small RNAs, EBER-1 and EBER-2 [7–9], which modulate the interferon-mediated antiviral response [10].

Adenoviruses (Ads) encode two kinds of non-coding small-RNAs, known as virus-associated (VA) RNAs, VAI and VAII, that consist of 157–160 nucleotides (nts). After Ad infection, the transcription of VA RNAs starts at the same time as the E1A gene and lasts until the late phase. Since the transcription level of VA RNAs increases depending on the number of viral genome copies, VA RNAs in Ad-infected cells are abundant during the late phase, and this is one reason why the functional analysis of VA RNAs during the late phase has been investigated much more frequently than during the early phase.

The VA RNA I (VAI), which is expressed at a level of $10^8$ copies per infected cell during the late phase [11], is required to establish efficient translation in virus-infected cells [12,13]. Moreover, it is well known that VAI inhibits anti-viral double-stranded RNA (dsRNA)-activated protein kinase (PKR). Also, VAI stabilizes ribosome-associated viral mRNAs, which could lead to enhanced levels of protein synthesis [14]. These findings have indicated that VAI plays a role in creating suitable conditions for viral growth, at

least during the late phase of infection. Recently, VA RNAs have been reported to be processed to microRNAs (mivaRNAs) via the cellular RNA-interference (RNAi) machinery, and mivaRNAs disturb cellular DNA expressions during the late phase [15]. However, it has not been investigated the function of VA RNA during the early phase, though the expression of VA RNAs starts immediately during the early phase of viral infection.

E1- and E3-deleted adenovirus vectors (AdVs), known as first-generation (FG) AdVs, have widely been used for the transient expression of transgenes in various cell types. FG AdVs lack E1A gene, an essential for viral replication; consequently, they neither express any viral gene product in target cells nor replicate except in 293 cells, which express E1A gene constitutively. However, since VA RNAs are transcribed by RNA polymerase III, their expressions are independent of E1A-mediated transactivation and they are always transcribed from AdV genome in AdV-infected cells. Therefore, FG AdVs are thought to be a suitable tool for the investigation of VA RNA function during the early phase of viral infection, since they express VA RNAs but do not replicate except in 293 cells. Moreover, these AdVs allow us to study the function of VA RNAs during both early and late phase using 293 cells. For this purpose, AdVs lacking VA RNA genes (VA-deleted AdVs) are essential as a control; however, VA-deleted AdVs have been difficult to generate and produce in quantities sufficient for practical use. Recently, we have developed a novel method for the efficient production of VA-deleted AdVs using a site-specific recombinase FLP [16]. A "pre-vector" containing the VA RNA region flanked by a pair of FRT sequences, which are target sequences for FLP recombinase, is constructed according to a commonly used method for the production of FG AdV [17]. This pre-vector, which is obtained at a high titer, is subsequently used to infect a 293 cell line that constitutively expresses humanized-FLPe [18] (293hde12) [19] so that the VA RNA region is removed from replicating viral genome. Since the excision efficiency of FLP in 293hde12 cells is high enough to remove almost all the VA RNA region from the very high number of viral genome copies, this method can be used to generate a high-titer of VA-deleted AdVs efficiently.

Here, we demonstrated the effect of VA RNAs expressed via FG AdVs on cellular gene expression by comparing the expression patterns between VA-deleted AdV- and FG AdV-infected cells using a microarray analysis. We found that VA RNAs expressed from FG AdVs disturbed the cellular gene expressions. Especially, the expression level of HDGF (hepatoma-derived growth factor; ENSG00000143321.14) was significantly decreased under the replication-deficient conditions; notably, HDGF expression started to decrease even during the early phase of infection in the 293 cells. Moreover, the overexpression of the HDGF gene inhibited viral growth in 293 cells, suggesting that the suppression of HDGF gene expression mediated by the VA RNAs was important for viral growth. This is the first report to show the function of VA RNAs during the early phase of infection.

## Materials and Methods

### Cells and AdVs

Human embryo kidney 293 cell line (ATCC) [20], human lung carcinoma A549 cell line (ATCC) [21], and human hepatocellular carcinoma derived HuH-7 cell line (RIKEN BRC) [22]were cultured in Dulbecco's modified Eagle's medium (DMEM) supplemented with 10% fetal calf serum (FCS). 293hde12 cell line [19], which is a 293 cell line possessing the hFLPe gene [18] (an improved version of the FLPe gene [23]), was cultured in DMEM supplemented with 10% FCS plus geneticin (0.75 mg/mL). After infection with AdVs, the cells were maintained in DMEM supplemented with 5% FCS without geneticin. For AraC (cytosine b-D-arabinofuranoside, hydrochloride: Sigma) treatment, the infected cells were maintained in DMEM supplemented with 5% FCS plus AraC (20 μg/mL).

The FG AdVs were prepared using 293 cells, which constitutively express adenoviral E1 genes and support the replication of E1-substituted AdVs. The VA-deleted AdVs except for HDGF- and GFP-expressing AdVs were prepared according to a method using 293U6VA-1 cells that constitutively express both VAI and VAII. HDGF-expressing and GFP-expressing VA-deleted AdVs were generated as described previously [16]. Briefly, an HDGF-expressing and a GFP-expressing unit under the control of the EF1α promoter was inserted into the SwaI cloning site at the authentic E1 substitution region in the pre-vector cosmid pAxdV-4FVF-w, and the pre-vectors were prepared using 293 cells. Subsequently, the pre-vectors were used to infect 293hde12 cells that constitutively express humanized FLPe recombinase [19] to excise the VA RNA region from the replicating viral genome. The VA-deleted AdVs transcribed less than 1% of the VA RNAs, compared with the FG AdVs, as confirmed using real-time PCR [16]. The VA-deleted AdVs and the FG AdVs were titrated using the methods described by Pei et al [24]. Briefly, the copy numbers of a viral genome that was successfully transduced into infected target cells were measured using qPCR (relative virus titer: rVT). This method enabled us to compare the various titers, since the transduction titer is not influenced by the growth rate of the 293 cells, even if an expressed gene product is deleterious to 293 cells.

### Plasmids

The pVA41da plasmid [16] contains a DNA fragment covering all of VAI and VAII from nt position 10576–11034 of adenovirus type 5. The pBluescript SK (-) (Stratagene) was used as a control. The plasmids were transfected using Transfast (Promega). A pxEFGFP plasmid expressing GFP under the control of the EF1α promoter was used as a transfection control. Two days after the transfection of pVA41da plasmid into 293 cells, the cells were harvested and the total RNAs were extracted as described below to measure the HDGF mRNA levels using qPCR.

### Microarray analysis

VA-deleted AdV (Axd12CARedE) and VA-containing FG AdV (AxCAdsRedE) were infected at an MOI (multiplicity of infection) of 0.5 to A549 cells for 24 h. We prepared triplicate samples for each of the conditions, and total RNA isolation was performed using a Qiagen RNeasy kit (Qiagen). A DNA microarray analysis using Affymetrix Gene-Chip technology was performed as described previously [25–27]. Briefly, 100 ng of total RNAs were used as a template for cDNA synthesis, and biotin-labeled cRNA was synthesized with a 3′ IVT Express Kit (Affymetrix). After generating the hybridization cocktails, hybridization to the DNA microarray (Genechip; Human Genome U133 Plus 2.0 Array; Affymetrix) [28] and fluorescent labeling were performed. The microarrays were then scanned with a GeneChip; Scanner 3000 7G System (Affymetrix). The data analysis was performed using GCOS software (Affymetrix). Signal detection and quantification were performed using the MAS5 algorithm with default settings. Global normalization was performed so that the average signal intensity of all the probe sets was equal to 100. For the clustering analysis, the signals were normalized and calculated to the individual scores, and the scores were visualized using Spotfire DecisionCite [29]. The analysis of variance among the groups was also performed using Spotfire DecisionCite and normalized data.

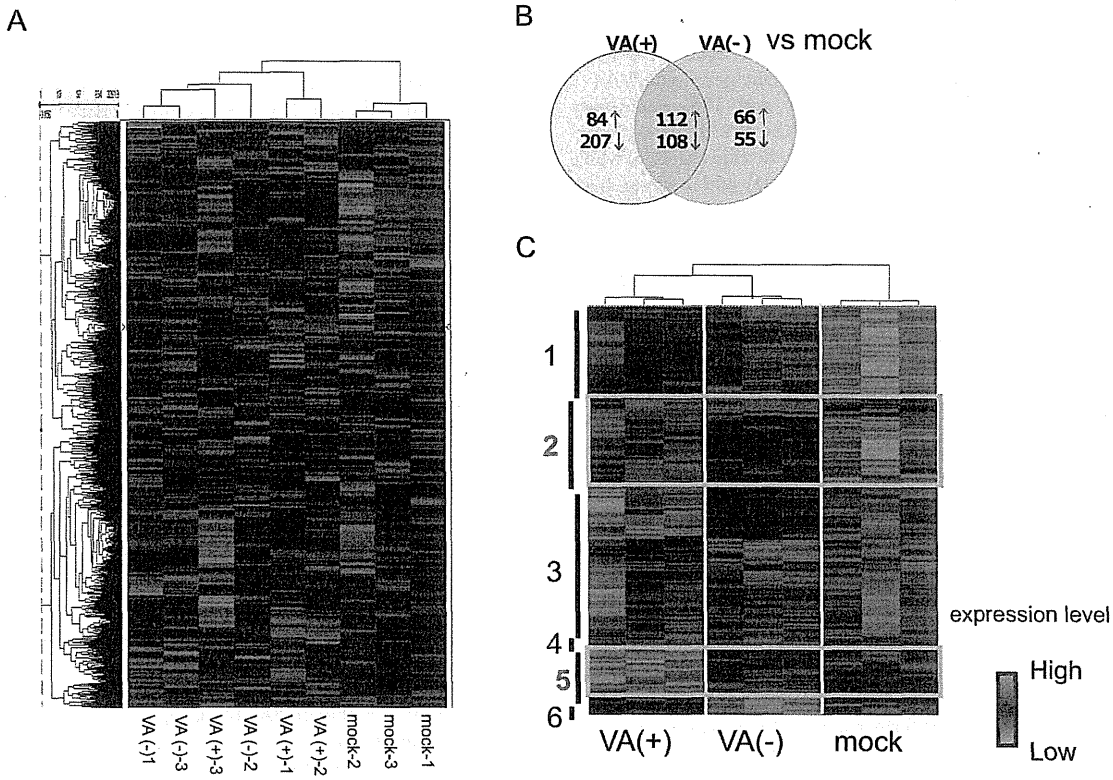


**Figure 1. Microarray analysis.** Global gene expression analysis of AdV infected A549 cells by Affymetrix microarray. Cells were harvested and total RNA was isolated after 24 h after infection. (A) Hierarchical clustering analysis using 32,619 genes of which expression was determined as "Present" in GCOS software in every sample. (B) The numbers of up or down regulated genes compared with mock infected group (Fold change >1.5, $P<0.01$). Red arrow indicates the numbers of up-regulated genes, and blue arrow indicates the numbers of down-regulated genes. (C) Identification and isolation of VA (+) specific gene clusters by hierarchical clustering analysis. The numbers of target genes were 2,800 genes, which were selected by ANOVA analysis in advance.
doi:10.1371/journal.pone.0108627.g001

All the data acquired by the microarray analysis were deposited in the NCBI Gene Expression Omnibus (NO. GSE58605).

### Quantitative real-time PCR

The total RNA of the infected cells was extracted, and the amount of expressed target RNA and 18S-rRNA (correction standard) were quantified using reverse-transcription and real-time PCR (Applied Biosystems Villa7); the ratio of the target RNA to 18S-rRNA was then calculated. To quantify the AdV genome, the infected total cell DNA was prepared from cells using a previously described method [30,31] or a DNA preparation kit (TaKaRa Bio). Quantitative PCR (qPCR) was performed to detect the AdV genome using a probe for the pIX gene, as described previously [24]. The amount of chromosomal DNA was simultaneously measured to correct the Ct values of the viral genome per cell. The probes were derived from the sequence of the human β-actin gene for HeLa and HuH-7 cell lines. The qPCR reaction was performed according to the manufacturer's protocol: 50°C for 2 min and 95°C for 10 min, followed by 40 cycles of 95°C for 15 sec and 60°C for 1 min (Applied BioSystems).

### Western blot analysis

Two days after transfection, 293 cells were harvested and the total protein was extracted using NP-40 lysis buffer [50 mM Tris-HCl (pH 8.0), 0.15M NaCl, 5 mM EDTA, 1% NP-40]. The lysates were mixed well in a rotator for 2 h at 4°C, centrifuged at 15,000 rpm for 5 min at 4°C, and the supernatants were collected. Western blotting was performed as described previously [32]. The membrane was incubated for 2 h at room temperature in the presence of anti-HDGF mouse monoclonal antibody (Bio Matrix Research, #BMR00572) diluted to 0.3 μg/mL with PBS-Tween, followed by incubation with peroxidase-conjugated goat anti-mouse IgG+IgM (Jackson Immunoresearch, #115-035-068) diluted to 1/10,000 with PBS-Tween. An anti-actin peptide goat polyclonal antibody (Santa Cruz Biotechnology, #sc-1616) diluted to 1/200 was also detected to show equal loading.

## Results

### HDGF gene expression was downregulated in FG-AdV infected cells

To determine whether VA RNAs expressed from FG AdVs disturb cellular gene expression, a microarray analysis was performed. We conducted a hierarchical clustering analysis using data for 32,619 genes, which were determined by GCOS software as being expressed in all the samples. The clusters were divided into two clear groups: namely, a mock group and an AdV-infected group (Figure 1A). Then, we conducted a pairwise comparison and drew a Venn diagram between the mock group vs. VA (−), i.e. VA-deleted AdV, and the mock group vs. VA (+), i.e. FG AdV,

according to the criteria of a 1.5-fold change (either an increase or a decrease) and $P<0.01$. In AdV-infected cells, more than 600 genes showed a significant increase/decrease against the mock cells in total. The numbers of VA-(+) specific genes and VA-(−) specific genes were found to be 300 and 100, respectively (Figure 1B). These results indicated that the VA RNAs expressed from AdV do not have a major impact on the expressions of whole genes. Using an ANOVA analysis ($P<0.01$) and a hierarchical clustering analysis, we isolated 6 gene clusters and 2,800 genes that showed different gene expressions between any of the group combinations. Among the 6 clusters, gene clusters 2 and 5 exhibited VA (+)-specific increases in gene expression and VA (+)-specific decreases in gene expression, respectively. According to this gene list (Table S1 in File S1) and literature survey, we finally selected several genes as targets for further research.

Next, we attempted to validate whether our microarray strategy was actually capable of identifying the targets of VA RNAs. We selected a subset of genes, all of which were upregulated or downregulated only after FG AdV infection and not after VA-deleted AdV infection, compared with the mock cells, and measured their transcript levels using quantitative RT-PCR (qPCR) in HeLa cells and HuH-7 cells. The results showed that the expression levels of some of these selected genes were actually changed in response to VA RNAs in both cell lines, except for the PTPRJ gene (Table 1). In contrast, we did not observe any significant changes in the transcript levels of TIA-1 (ENSG00000116001.11), which have been identified as a target for mivaRNA, a microRNA derived from VA RNA [15]. We chose the HDGF gene for further analysis since its transcript was remarkably decreased in both cell lines when FG AdVs were infected.

## HDGF gene expression was suppressed by a lower level of VA RNAs than TIA-1

To examine whether the VA RNAs expressed from a plasmid also suppress HDGF gene expression, a VA-RNA expressing-plasmid, pVA41da [16], was transfected into 293 cells. Two days later, the total cellular RNA and protein were collected and HDGF expression was measured at the transcript level using qPCR (Figure 2A) and at the protein level using a western blot analysis (Figure 2B), respectively. The result showed that HDGF mRNA was significantly decreased, even in cells with a low level of VA-RNA transduction (Figure 2A, HDGF, 0.1 μg/well), in comparison with control plasmid-transduced cells (Figure 2A, HDGF, 0). In contrast, no significant change in TIA-1 expression was observed in the low VA RNA transduced cells (Figure 2A, TIA-1, 0.1 and 0.25), and it was suppressed only in the highest VA RNA-transduced cells (Figure 2A, TIA-1, 0.5). HDGF suppression mediated by VA RNA was also detected at the protein level (Figure 2B). The HDGF protein was significantly decreased in cells that had been transfected with the VA RNA-expressing plasmid (Figure 2B, lane 2, VA (+)), compared with the mock cells (lane 1, mock) or the control plasmid-transduced cells (lane 3, VA (−)). The suppression of HDGF transcript was also observed in VA RNA-expressing 293 cell lines named 293VA1 and 293VA42 [33], compared with that in the parent 293 cells (Table S2 in File S1). Therefore, VA RNAs suppressed HDGF expression under the conditions other than viral infection, and a smaller amount of VA RNA than TIA-1 was sufficient to suppress HDGF.

## HDGF gene expression was suppressed during the early phase of viral infection

To determine the period during which HDGF was downregulated in the adenovirus life cycle, the VA-deleted AdVs and the FG-AdVs were used to infect 293 cells at an MOI of 5. Then, the cellular RNA was isolated to measure the HDGF transcript levels using qPCR at the indicated time points (Figure 3). The VA-deleted AdVs and the FG-AdVs are structurally identical except for their VA RNA expression, and these E1-deleted vectors are able to replicate in 293 cells because the E1 proteins are supplied *in trans*. The results showed that the transcript levels of HDGF started to decrease at 8 h after infection (early phase) in FG AdV-infected cells (Figure 3A, white circle). Interestingly, after VA-deleted AdV infection, the HDGF level clearly increased above the basal level at 8 h (Figure 3A, black square). This induction of HDGF expression after VA-deleted AdV infection was also observed under replication-deficient conditions in HuH-7 cells (Figure S1 in File S1, bars 1 and 3). In contrast, the TIA-1 mRNA level was similar to the basal level at 8 h and it obviously decreased to comparable level with HDGF only at 16 h (late phase) after FG-AdV infection (Figure 3B, white circle), whereas no significant upregulation was observed after VA-deleted AdV infection (Figure 3B, black square). Since the replication of the viral genome occurs at around 8 h after infection, these results showed that the suppression of HDGF and TIA-1 began during the early and late phases of viral infection, respectively. The results for TIA-1 suppression using AdVs were consistent with those of a previous report indicating that TIA-1 is downregulated during the late phase of infection with wild-type adenovirus [15]. We further examined the point that the HDGF level increased to more than 125% of the steady-state level at 8 h after VA-deleted AdV infection (Figure 3A), though the TIA-1 level did not (Figure 3B).

**Table 1.** Changes in expression levels of cellular genes in response to VA RNAs.

| gene | ratio VA(+)/VA(−) | |
|---|---|---|
| | HuH-7 | HeLa |
| PAPPA | 1.23 | 1.60 |
| PTPRJ | 1.09 | 1.06 |
| STS1-3 | 0.82 | 0.80 |
| HDGF | 0.43 | 0.65 |
| TIA-1 | 1.10 | 1.09 |

Each mRNA level in the HuH-7 cells and HeLa cells was quantified using qPCR, and the ratio of the expression level in FG AdV infected cells (VA (+)) compared with that in VA-deleted AdV infected cells (VA (−)) was calculated.

doi:10.1371/journal.pone.0108627.t001